European Journal of Mechanics / A Solids 90 (2021) 104357

Contents lists available at ScienceDirect

European Journal of Mechanics / A Solids

journal homepage: www.elsevier.com/locate/ejmsol

A natural vector/matrix notation applied in an efficient and robust return-mapping algorithm for advanced yield functions

Tomáš Mánik

Department of Materials Science and Engineering, Norwegian University of Science and Technology, Alfred Getz vei 2, 7491, Trondheim, Norway

ARTICLE INFO

Keywords:
Continuum plasticity
Plastic anisotropy
Yield function
Return mapping algorithm
Vector notation

ABSTRACT

A fast and robust stress-integration algorithm is the key to full exploitation of advanced anisotropic yield functions in computational mechanics. Poor global convergence of a direct application of the Newton-Raphson scheme has been rectified by applying line search strategies during the Newton iterations. In this work the line-search approach is further improved by a better first guess. The new algorithm is implemented into a user-defined material subroutine (UMAT) in a finite-element (FE) software and tested. The implementation is made easier and more efficient by a new advantageous vector/matrix notation for symmetric second- and fourth-order tensors, which is the second result of this work. Benefits of this notation are discussed with respect to formulation of continuum-plasticity models as well as their implementations. FE simulations were run to demonstrate the performance of the new implementation, which is available as open-source software via GitLab repository (see Appendix). The new return-mapping algorithm implementation runs equally fast and robust as the simple von Mises and Hill standard implementations in the Abaqus/Standard software. This enables full exploitation of advanced yield functions as the new standard in industrial FE applications.

1. Introduction

In order to solve boundary value problems for an elasto-plastic body by computational solid mechanics codes, constitutive equations need to be numerically integrated. As stated by Hughes (1984), the local integration of constitutive equations is the central problem of computational plasticity. Due to the large difference between the elastic and plastic behavior, there is an inherent lack of smoothness, requiring a robust algorithm. Many different methodologies have been developed to numerically integrate the constitutive equations over an increment. In finite element codes the most used method for stress integration is the predictor-corrector method commonly referred as the return-mapping algorithm, introduced by (Wilkins, 1969). For the simplest and mathematically most convenient von Mises yield surface, the simple radial return-map can be used. Many extensions of the original algorithm have been made to account for more complex plasticity models, see e.g. Nagtegaal (1982), Simo and Ortiz (1985), Ortiz and Popov (1985), Ortiz and Simo (1986), Simo et al. (1988).

The quadratic nature of the anisotropic Hill48 model (Hill, 1948) allows for specific return-mapping algorithms to be employed (De Borst and Feenstra, 1990; Maudlin et al., 1999; Versino and Bennett, 2018). Due to its simplicity, Hill48 is the most used yield surface for orthotropic metals, especially steels. However, it has limitations for highly anisotropic metals, such as aluminium alloys. When more advanced, non-quadratic yield functions are used, no simple algorithm exists for obtaining the implicit time stepping. The semi-implicit return-map (Moran et al., 1990), the cutting-plane method (Ortiz and Simo, 1986), a quasi-implicit or the fully implicit backward-Euler algorithm are commonly used. Description of the principal methods is given in text-books e.g. by Simo and Hughes (1998) and Dunne and Petrinic (2006). Extensive literature review of integration procedures used in a finite element method is given by (Kojić, 2002). See a comparison study of distinct algorithms for complex non-quadratic models by Grilo et al. (2014). Other examples of more recent approaches are works by Mosler and Bruhns (2010), Becker (2011), Scherzinger (2017), Lester and Scherzinger (2017) and Choi and Yoon (2019), among others.

The stability and accuracy of the return-mapping algorithm may limit the time step which, consequently, affect the computational efficiency of simulations. The unconditionally stable fully implicit backward-Euler return-mapping algorithm is typically combined with a Newton-Raphson iterative process (Simo and Hughes, 1998). However, when applied to Hosford (1972) or Yld2004-18p yield surface (Barlat et al., 2005), this algorithm is shown to diverge for large number of trial stresses (Scherzinger, 2017). When a line-search is added to the

E-mail address: tomas.manik@ntnu.no.

https://doi.org/10.1016/j.euromechsol.2021.104357
Received 9 January 2021; Received in revised form 18 May 2021; Accepted 25 June 2021
Available online 1 July 2021

Newton-Raphson iterations, the return-mapping algorithm is shown to gain excellent effectiveness and robustness (Pérez-Foguet and Armero, 2002; Scherzinger, 2017; Soare and Barlat, 2011). Good convergence was achieved even for very large trial stress states. Besides the line-search, another strategies e.g. a multi-step Newton Raphson has been applied to enhance the convergence of the implicit backward Euler return-mapping algorithm (Lee et al., 2012).

In each Newton iteration, both the gradient and the Hessian of the yield function, being second- and fourth-order tensors, respectively, need to be computed. Several algebraic operations involving inversions, outer and inner products of second- and fourth-order tensors need to be performed. The return-mapping algorithm for complex plasticity models easily becomes a computationally expensive part of the simulation. For this reason, a reduced vector/matrix representation of symmetric tensorial quantities is commonly utilized in the return-mapping algorithms as it considerably reduces the computational cost.

The numerical solution of equations involving higher order tensors, in practice requires a conversion into solving a linear algebra problem. Symmetric second-order tensors and fourth-order tensors with minor symmetry can be mapped into a vector and matrix representation, respectively. Voigt and Mandel representations (or notations) are the most widely used. Such compressed representation exploits the tensor symmetries and thus significantly reduces number of operations and the computation cost. This is taken advantage of in implementations of computational mechanics.

The Voigt notation suffers from that its tensor components correspond to a non-normalized basis, making distinction of covariant and contravariant coordinates necessary (Helnwein, 2001). Hence, the Voigt notation is different for stress-like and strain-like tensors, which are stored in contravariant and covariant Voigt forms, respectively. This has consequences for manipulations with minor-symmetric fourth-order tensors in Voigt form. For example, the inverse of the Voigt contravariant matrix does not lead to a contravariant Voigt matrix, but to a covariant matrix and vice versa. Thus, obtaining the inverse of a matrix in a Voigt notation requires pre- or post-multiplications or divisions of some components of the matrices with factors of 2 and 4 (Brannon, 2018). This can make calculations using Voigt notation error prone.

The Mandel notation does not have this inconvenience associated with the Voigt notation. Applying an orthonormal basis, there is no distinction between covariant and contravariant components, hence stress- and strain-like tensors transform equally. For instance, Mandel components of the inverse fourth-order tensor $\mathbb{A}^{-1}$ are found simply by inverting the Mandel 6x6 matrix $\mathbf{A}$.

The plastic response of metallic materials is classically considered as independent of the hydrostatic pressure. The yield function is thus a function of a deviatoric stress tensor, and its first and second derivatives with respect to the hydrostatic pressure equal zero. The latter is exploited neither when Voigt nor the Mandel notation is employed to calculate the yield function gradient $\partial_{\boldsymbol{\sigma}} f$ or Hessian $\partial^2_{\boldsymbol{\sigma}\boldsymbol{\sigma}} f$, as 6x1 and 6x6 arrays, respectively. Hence, for each iteration in the return-map, the Jacobian $\boldsymbol{\Xi} = \left(\mathbf{C}^{-1} + \Delta\gamma\, \partial^2_{\boldsymbol{\sigma}\boldsymbol{\sigma}} f\right)^{-1}$ (Simo and Hughes, 1998), needs to be computed by solving a linear system of 6 equations. However, since the plastic-corrector part of the return-map is independent on the hydrostatic pressure, the latter can entirely be omitted from the iterative process. This can be done by constructing an alternative vector/matrix representation that contains the volumetric and deviatoric parts of the second-order tensor explicitly in its mapping. This will reduce the dimension of equation system from 6 to 5, as the Jacobian in the Newton iterations as part of the return-map will become a 5x5 matrix. When reducing the system dimension from $n = 6$ to 5, the resulting linear equation system solved by the Cholesky decomposition involving $\frac{2}{3}n^3$ operations, will take about 60% of the time, and a matrix inversion about 43%, which will contribute to a lower computing time.

An orthonormal basis that separates the hydrostatic pressure was found by Kocks et al. (1998), when studying elastic tensor properties of crystals with cubic symmetry. It was denoted as a natural basis for formulating crystal plasticity. However, only the deviatoric part was used in the self-consistent modelling of heterogeneous plasticity in the VPSC - Visco-plastic self-consistent) code (Lebensohn and Tomé, 1993).

In this paper, application of the natural notation in continuum plasticity is presented. This notation has an orthonormal basis, so it has all the convenient properties of the Mandel notation. Moreover, due to explicit representation of the deviator, the natural notation is advantageous for expressing symmetric second- and fourth-order tensors in continuum plasticity and suits both pressure-dependent and independent yield criteria.

The paper starts by reviewing the existing notations. Then, the natural notation and the associated transformation matrices are presented. Matrix representation of elastic and plastic fourth-order tensors, specifically elastic stiffness and compliance moduli as well as plastic von Mises, Hill and Barlat anisotropic tensors are shown. Finally, application of the natural notation in an efficient and robust return-mapping algorithm with Yld2004-18p yield function recently developed by Scherzinger (2017) is presented. Significant convergence improvement by introducing a radial-return predictor instead of the elastic predictor is demonstrated with FE simulations of a uniaxial compression and tension using user-defined material subroutine (UMAT) in the Abaqus/Standard 2020.

2. Existing notations

In order to describe physical phenomena related to mechanics of solids, use of scalar, vectoral and tensorial quantities of various order are required. Within the classical continuum and crystal plasticity theories, tensors of second order are necessary for description of stresses, displacement gradients, yield function gradients and various state-dependent variables, fourth-order tensors are needed for expressing the elastic stiffness tensor, the elasto-plastic tangent modulus, the acoustic tensor, plastic anisotropic tensors (Barlat et al., 2005) or various state-dependent tensors representing directional hardening of the material (Levkovitch and Svendsen, 2007). Third-, fifth- and sixth-order tensors are required in e.g. higher-order continuum theories (Auffray et al., 2013).

Assume a real 3-dimensional vector space, where $\boldsymbol{e}_1$, $\boldsymbol{e}_2$ and $\boldsymbol{e}_3$ are orthonormal vectors defining an orthonormal basis $\{\boldsymbol{e}_i\}_{i=1,\dots,3}$. Then a vector $\boldsymbol{u}$, a second-order tensor $\boldsymbol{A}$ and a fourth-order tensor $\mathbb{C}$ can be represented as $\boldsymbol{u} = u_i \boldsymbol{e}_i$, $\boldsymbol{A} = A_{ij} \boldsymbol{e}_i \otimes \boldsymbol{e}_j$, and $\mathbb{C} = C_{ijkl} \boldsymbol{e}_i \otimes \boldsymbol{e}_j \otimes \boldsymbol{e}_k \otimes \boldsymbol{e}_l$, where the scalars u_i, A_{ij} and C_{ijkl} are the components of $\boldsymbol{u}$, $\boldsymbol{A}$ and $\mathbb{C}$, respectively, with respect to the basis $\{\boldsymbol{e}_i\}_{i=1,\dots,3}$. The Einstein convention for repeated indices is employed throughout the paper. In addition, the orthonormal basis will solely be used and, accordingly, all the vectors and tensors will be Cartesian.

2.1. Voigt notation

It is possible to represent second- and fourth-order tensors in a given vector space by a vector and second-order tensor, respectively, but in another vector space with higher dimension (Moakher, 2008). Such order reduction of a tensor allows more efficient tensor manipulation. The original reduced representation was suggested by Voigt (1910) and applied within the elasticity theory. For a symmetric tensor, Voigt has chosen to arrange first the normal components, followed by shear components. In order to preserve work conjugacy, a factor of 2 had to be

introduced for the shear strain components when written in vector Voigt form. Voigt notation thus makes distinction between a stress-like and a strain-like tensor as

$$\boldsymbol{\sigma} = \begin{pmatrix} \sigma_{11} & \sigma_{12} & \sigma_{13} \\ \sigma_{12} & \sigma_{22} & \sigma_{23} \\ \sigma_{13} & \sigma_{23} & \sigma_{33} \end{pmatrix} \rightarrow \boldsymbol{\sigma}^V = \begin{pmatrix} \sigma_{11} \\ \sigma_{22} \\ \sigma_{33} \\ \sigma_{23} \\ \sigma_{13} \\ \sigma_{12} \end{pmatrix}$$

and

$$\boldsymbol{\varepsilon} = \begin{pmatrix} \varepsilon_{11} & \varepsilon_{12} & \varepsilon_{13} \\ \varepsilon_{12} & \varepsilon_{22} & \varepsilon_{23} \\ \varepsilon_{13} & \varepsilon_{23} & \varepsilon_{33} \end{pmatrix} \rightarrow \boldsymbol{\varepsilon}^V = \begin{pmatrix} \varepsilon_{11} \\ \varepsilon_{22} \\ \varepsilon_{33} \\ 2\varepsilon_{23} \\ 2\varepsilon_{13} \\ 2\varepsilon_{12} \end{pmatrix} \tag{1}$$

Note, that the order of the shear components varies in the literature, plasticity books and finite element codes. Throughout this paper, the order given in Eq. (1) will be used. This coincides with the order originally used by Voigt (1910) and further adopted e.g. by Barlat et al. (2005), Aretz et al. (2010) and Aretz and Barlat (2013) for defining the anisotropic transformation matrices as part of the yield functions Yld2004-18p, Yld2004-27p and Yld2011-18p. As an example, the sequence 12-13-23 is used by Abaqus/Standard, whereas the sequence 12-23-13 is applied in Abaqus/Explicit, MSC. Marc, LS-DYNA and ANSYS.

The Voigt notation preserves work conjugacy as the inner product between stress and strain tensors, which turns into a dot-product of their Voigt vector representations, e.g. $W = \boldsymbol{\sigma} : \boldsymbol{\varepsilon} = (\boldsymbol{\sigma}^V)^{\mathrm{T}}\, \boldsymbol{\varepsilon}^V$. Note, however, that this equality does not hold for the inner product between two stress or strain tensors, as e.g. $\boldsymbol{\sigma} : \boldsymbol{\sigma} \neq (\boldsymbol{\sigma}^V)^{\mathrm{T}}\, \boldsymbol{\sigma}^V$ or $\boldsymbol{\varepsilon} : \boldsymbol{\varepsilon} \neq (\boldsymbol{\varepsilon}^V)^{\mathrm{T}}\, \boldsymbol{\varepsilon}^V$. Adjustments by a factor of 2 in the multiplication of the shear components are required.

Helnwein (2001) pointed out that the compressed vector representation can be, in general, identified as a mapping with covariant, contravariant or mixed-variant coordinates of a non-orthonormal basis in a six-dimensional vector space. The Voigt notation is a mapping with a non-orthonormal basis and has a covariant and a contravariant basis that do not coincide. More details can be found in Helnwein (2001) and Brannon (2018). A symmetric second-order stress tensor $\boldsymbol{\sigma}$ (contravariant) and strain tensor $\boldsymbol{\varepsilon}$ (covariant) are both represented by a 6-dimensional vector but with a different basis. Written in the indicial notation,

$$\begin{aligned} \boldsymbol{\sigma} &= \sigma_{ij} \boldsymbol{e}_i \otimes \boldsymbol{e}_j = \sigma_i^V \boldsymbol{E}_{\sigma i}^V \\ \boldsymbol{\varepsilon} &= \varepsilon_{ij} \boldsymbol{e}_i \otimes \boldsymbol{e}_j = \varepsilon_i^V \boldsymbol{E}_{\varepsilon i}^V \end{aligned} \tag{2}$$

where $\{\boldsymbol{E}_{\sigma i}^V\}_{i=1,\dots,6}$ and $\{\boldsymbol{E}_{\varepsilon i}^V\}_{i=1,\dots,6}$ are two orthogonal sets of the Voigt bases, listed as

$$\begin{aligned} \boldsymbol{E}_{\sigma 1}^V &= \boldsymbol{E}_{\varepsilon 1}^V = \boldsymbol{e}_1 \otimes \boldsymbol{e}_1 & \boldsymbol{E}_{\sigma 4}^V &= \frac{1}{2}\boldsymbol{E}_{\varepsilon 4}^V = \boldsymbol{e}_2 \otimes \boldsymbol{e}_3 + \boldsymbol{e}_3 \otimes \boldsymbol{e}_2 \\ \boldsymbol{E}_{\sigma 2}^V &= \boldsymbol{E}_{\varepsilon 2}^V = \boldsymbol{e}_2 \otimes \boldsymbol{e}_2 & \boldsymbol{E}_{\sigma 5}^V &= \frac{1}{2}\boldsymbol{E}_{\varepsilon 5}^V = \boldsymbol{e}_1 \otimes \boldsymbol{e}_3 + \boldsymbol{e}_3 \otimes \boldsymbol{e}_1 \\ \boldsymbol{E}_{\sigma 3}^V &= \boldsymbol{E}_{\varepsilon 3}^V = \boldsymbol{e}_3 \otimes \boldsymbol{e}_3 & \boldsymbol{E}_{\sigma 6}^V &= \frac{1}{2}\boldsymbol{E}_{\varepsilon 6}^V = \boldsymbol{e}_1 \otimes \boldsymbol{e}_2 + \boldsymbol{e}_2 \otimes \boldsymbol{e}_1 \end{aligned} \tag{3}$$

A fourth-order tensor, $\mathbb{C}$, with minor symmetry, i.e. $C_{ijkl} = C_{jikl} = C_{ijlk} = C_{jilk}$ is represented in Voigt notation as a 6x6 matrix as

$$\mathbf{C}^V = \begin{pmatrix} C_{1111} & C_{1122} & C_{1133} & C_{1123} & C_{1113} & C_{1112} \\ C_{2211} & C_{2222} & C_{2233} & C_{2223} & C_{2213} & C_{2212} \\ C_{3311} & C_{3322} & C_{3333} & C_{3323} & C_{3313} & C_{3312} \\ C_{2311} & C_{2322} & C_{2333} & C_{2323} & C_{2313} & C_{2312} \\ C_{1311} & C_{1322} & C_{1333} & C_{1323} & C_{1313} & C_{1312} \\ C_{1211} & C_{1222} & C_{1233} & C_{1223} & C_{1213} & C_{1212} \end{pmatrix} \tag{4}$$

In general, a fourth-order tensor $\mathbb{C}$ represents a linear map that assigns to each second-order tensor $\boldsymbol{A}$ the second-order tensor $\mathbb{C} : \boldsymbol{A}$, written in the indicial notation as $C_{ijkl}A_{kl}$. Due to the existence of dual bases and distinction between stress-like and strain-like tensors, the representation of a fourth-order tensor differs depending on whether it maps e.g. a strain tensor to a stress tensor, or a stress tensor to a strain tensor. Examples of the former and latter mapping are the elastic stiffness tensor $\mathbb{C}$ and the compliance tensor $\mathbb{S}$, respectively, which are expressed using the Voigt bases from Eq. (3) as

$$\mathbb{C} = C_{ij}^V \boldsymbol{E}_{\sigma i}^V \otimes \boldsymbol{E}_{\sigma j}^V \quad \text{and} \quad \mathbb{S} = S_{ij}^V \boldsymbol{E}_{\varepsilon i}^V \otimes \boldsymbol{E}_{\varepsilon j}^V \tag{5}$$

Hence, caution must be taken when performing algebraic operations. An example is Hooke's law, in which a product of a fourth-order elastic stiffness tensor and a second-order strain tensor, $\boldsymbol{\sigma} = \mathbb{C} : \boldsymbol{\varepsilon}$, or $\sigma_{ij} = C_{ijkl}\varepsilon_{kl}$ turns nicely into a matrix-vector multiplication $\boldsymbol{\sigma}^V = \mathbf{C}^V\, \boldsymbol{\varepsilon}^V$, where the matrix $\mathbf{C}^V$ is the Voigt representation of $\mathbb{C}$ according to Eq. (4). However, the inverse Hooke's law, $\boldsymbol{\varepsilon} = \mathbb{S} : \boldsymbol{\sigma}$, or $\varepsilon_{ij} = S_{ijkl}\sigma_{kl}$ cannot straightforward be calculated in Voigt notation with coefficients of the matrix $\mathbf{S}^V$ obtained by Eq. (4), i.e. $\boldsymbol{\varepsilon}^V \neq \mathbf{S}^V \boldsymbol{\sigma}^V$. Post-adjustments by factors 2 and 4 of shear components in the matrix $\mathbf{S}^V$are required. Different adjustments are necessary for cases when a fourth-order tensor represents mapping between two stress-like tensors (e.g. plastic anisotropic Hill's tensor, see Section 4.3, and between two strain-like tensors (needed during the Newton iterations in the return-mapping algorithm). An outer product between two stress-like tensors $\boldsymbol{A}$ and $\boldsymbol{B}$ as, $\mathbb{C} = \boldsymbol{A} \otimes \boldsymbol{B}$, or $C_{ijkl} = A_{ij}B_{kl}$ is in Voigt notation simply calculated as the outer product of two Voigt vectors as, $\mathbf{C}^V = \mathbf{a}^V(\mathbf{b}^V)^{\mathrm{T}}$, where $\mathbf{C}^V$ is the Voigt representation of $\mathbb{C}$ according to Eq. (4). However, post-adjustments of shear components in matrix $\mathbf{C}^V$ are required if $\boldsymbol{A}$ or $\boldsymbol{B}$ is a strain-like tensor. Citing Brannon (2018): "Deducing how to properly perform these adjustments is difficult, tedious and error-prone."

The Voigt notation is considered as the standard, as it is used for expressing the anisotropic elastic and plastic tensors for general material symmetries and it is utilized in implementations of numerical software for computational mechanics.

2.2. Mandel (or Voigt-Mandel) notation

The inconveniences with the Voigt notation do not exist in the Mandel (sometimes denoted as Voigt-Mandel) notation, which has an orthonormal basis and maps any symmetric second-order tensor equally as

$$\mathbf{A} = \begin{pmatrix} A_{11} & A_{12} & A_{13} \\ A_{12} & A_{22} & A_{23} \\ A_{13} & A_{23} & A_{33} \end{pmatrix} \rightarrow \mathbf{a}^M = \begin{pmatrix} A_{11} \\ A_{22} \\ A_{33} \\ \sqrt{2}A_{23} \\ \sqrt{2}A_{13} \\ \sqrt{2}A_{12} \end{pmatrix} \tag{6}$$

This notation was applied and extensively used by Mandel (1965), however, it must be noted that the multiplication of the shear stress components by the $\sqrt{2}$ factors was already suggested by Voigt (1910) (page 139). The Mandel representation is based on an orthonormal basis $\{\boldsymbol{E}_i^M\}_{i=1,\dots,6}$ constructed as

$$\begin{aligned} \boldsymbol{E}_1^M &= \boldsymbol{e}_1 \otimes \boldsymbol{e}_1 & \boldsymbol{E}_4^M &= \frac{1}{\sqrt{2}}(\boldsymbol{e}_2 \otimes \boldsymbol{e}_3 + \boldsymbol{e}_3 \otimes \boldsymbol{e}_2) \\ \boldsymbol{E}_2^M &= \boldsymbol{e}_2 \otimes \boldsymbol{e}_2 & \boldsymbol{E}_5^M &= \frac{1}{\sqrt{2}}(\boldsymbol{e}_1 \otimes \boldsymbol{e}_3 + \boldsymbol{e}_3 \otimes \boldsymbol{e}_1) \\ \boldsymbol{E}_3^M &= \boldsymbol{e}_3 \otimes \boldsymbol{e}_3 & \boldsymbol{E}_6^M &= \frac{1}{\sqrt{2}}(\boldsymbol{e}_1 \otimes \boldsymbol{e}_2 + \boldsymbol{e}_2 \otimes \boldsymbol{e}_1) \end{aligned} \tag{7}$$

A symmetric second-order tensor $\boldsymbol{A}$ and a fourth-order tensor $\mathbb{C}$ with minor symmetry are then expressed as $\boldsymbol{A} = a_i^M \boldsymbol{E}_i^M$ and $\mathbb{C} = C_{ij}^M \boldsymbol{E}_i^M \otimes \boldsymbol{E}_j^M$,

respectively.

Transformation of stress and strain from Voigt to Mandel notation can be done simply as

$$\boldsymbol{\sigma}^M = \mathbf{T}_\sigma^{V\to M}\,\boldsymbol{\sigma}^V \quad \text{and} \quad \boldsymbol{\varepsilon}^M = \mathbf{T}_\varepsilon^{V\to M}\,\boldsymbol{\varepsilon}^V, \tag{8}$$

respectively, in which $\mathbf{T}_\sigma^{V\to M}$ and $\mathbf{T}_\varepsilon^{V\to M}$ are 6x6 transformation matrices with the non-zero elements $(T_\sigma)_{11} = (T_\sigma)_{22} = (T_\sigma)_{33} = 1$ and $(T_\sigma)_{44} = (T_\sigma)_{55} = (T_\sigma)_{66} = \sqrt{2}$, and $\mathbf{T}_\varepsilon^{V\to M} = (\mathbf{T}_\sigma^{V\to M})^{-1}$. The Mandel notation also preserves the work conjugacy as the L_2-norm is preserved as, $\boldsymbol{A} : \boldsymbol{A} = (\mathbf{a}^M)^{\mathrm{T}}\,\mathbf{a}^M$.

Transformation of a fourth-order elastic stiffness tensor $\mathbb{C}$ from Voigt to Mandel notation is

$$\mathbf{C}^M = \mathbf{T}_\sigma^{V\to M}\mathbf{C}^V\left(\mathbf{T}_\varepsilon^{V\to M}\right)^{-1} = \mathbf{T}_\sigma^{V\to M}\,\mathbf{C}^V\,\mathbf{T}_\sigma^{V\to M} \tag{9}$$

The inverse of the fourth-order tensor $\mathbb{C}$ in the Mandel notation is simply the inverse of the Mandel matrix $(\mathbf{C}^M)^{-1}$. Any product as $\mathbb{C} : \boldsymbol{A}$ equals in Mandel notation to a matrix-vector product $\mathbf{C}^M\mathbf{a}^M$, and an outer product $\boldsymbol{A} \otimes \boldsymbol{A}$ is in Mandel notation simply the outer product $\mathbf{a}^M(\mathbf{a}^M)^{\mathrm{T}}$.

2.3. The 5-dimensional deviatoric notations

Vector representations for both stress and strain were introduced in crystal plasticity models without elasticity, originating from the Sachs and the Taylor-Bishop-Hill model (Bishop and Hill, 1951; Taylor, 1938) the further developed self-consistent models, and grain-cluster models as Lamel (Van Houtte et al., 1999), Alamel (Van Houtte et al., 2005), Alamel with an additional relaxation (Mánik and Holmedal, 2013) and GIA (Crumbach et al., 2001). Since only the deviatoric part of both the stress and plastic strain rate tensors enters the constitutive equations, the second- and fourth-order tensors can be represented, instead of 6-, by a 5-dimensional vector and a 5x5 matrix, respectively. The first 5-dimensional notation was suggested by Kocks et al. (1983) who, similarly to Voigt, used different vector representations for the deviatoric stress tensor $\boldsymbol{\sigma}'$ and the plastic strain-rate, reading

$$\boldsymbol{\sigma}^K = \begin{pmatrix} (\sigma'_{11} - \sigma'_{22})/2 \\ 3/2\sigma'_{33} \\ \sigma'_{23} \\ \sigma'_{13} \\ \sigma'_{12} \end{pmatrix}, \quad \dot{\boldsymbol{\varepsilon}}^{pK} = \begin{pmatrix} \dot{\varepsilon}^p_{11} - \dot{\varepsilon}^p_{22} \\ \dot{\varepsilon}^p_{33} \\ 2\dot{\varepsilon}^p_{23} \\ 2\dot{\varepsilon}^p_{13} \\ 2\dot{\varepsilon}^p_{12} \end{pmatrix} \tag{10}$$

This notation is implemented in the LApp v6.8 - Los Alamos polycrystal plasticity code (Kocks et al., 1995), which operates on the deviatoric components only. A slightly different notation was chosen by Tomé and Kocks (1985), as it was more suitable for the study of the yield surface of HCP crystals, reading

$$\boldsymbol{\sigma}^{TK} = \begin{pmatrix} 3(\sigma'_{11} + \sigma'_{22}) \\ \sigma'_{11} - \sigma'_{22} \\ \sigma'_{23} \\ \sigma'_{13} \\ \sigma'_{12} \end{pmatrix}, \quad \dot{\boldsymbol{\varepsilon}}^{pTK} = \begin{pmatrix} \left(\dot{\varepsilon}^p_{11} + \dot{\varepsilon}^p_{22}\right)/2 \\ \left(\dot{\varepsilon}^p_{11} - \dot{\varepsilon}^p_{22}\right)/2 \\ 2\dot{\varepsilon}^p_{23} \\ 2\dot{\varepsilon}^p_{13} \\ 2\dot{\varepsilon}^p_{12} \end{pmatrix} \tag{11}$$

Canova et al. (1985) concluded, that with respect to symmetries associated with hexagonal crystals, the five independent stress components should be defined as

$$\boldsymbol{\sigma}^{TK} = \begin{pmatrix} \dfrac{\sigma'_{11} + \sigma'_{22}}{2} & \dfrac{\sigma'_{11} - \sigma'_{22}}{2} & \sigma_{23} & \sigma_{13} & \sigma_{12} \end{pmatrix} \tag{12}$$

The first deviatoric notation that is common for any symmetric deviatoric second-order tensor $\boldsymbol{A}$, was suggested by Lequeu (1986). It reads

$$\mathbf{a}^L = \begin{pmatrix} (A_{22} - A_{11})/\sqrt{2} \\ \sqrt{3/2}\,(A_{11} + A_{22}) \\ \sqrt{2}A_{23} \\ \sqrt{2}A_{13} \\ \sqrt{2}A_{12} \end{pmatrix} \tag{13}$$

Lequeu derived this notation in order to simplify the plotting procedure, as the first two vector-components in this representation directly lead to the π-plane projection and other stress space cross-sections of suitable shape. The plastic work conjugacy came to his surprise as a bonus, as he mentions it as "an interesting consequence". The same notation, although independently obtained, is used in the VPSC code (Tome and Lebensohn, 2009).

Later, Van Houtte (1988) has chosen similar vector representation as by Lequeu (1986), reading

$$\mathbf{a}^H = \begin{pmatrix} \dfrac{\left(\sqrt{3}+1\right)A_{22} + \left(\sqrt{3}-1\right)A_{33}}{2} \\ \dfrac{\left(\sqrt{3}-1\right)A_{22} + \left(\sqrt{3}+1\right)A_{33}}{2} \\ \sqrt{2}A_{23} \\ \sqrt{2}A_{13} \\ \sqrt{2}A_{12} \end{pmatrix} \tag{14}$$

3. The natural basis applied to elasto-plastic problems

Note, that all the deviatoric, i.e. 5-dimensional vector notations, as introduced by Kocks et al. (1983), Tomé and Kocks (1985), Lequeu (1986) and Van Houtte (1988), preserve the plastic work-rate conjugacy, but only the latter two preserve the L_2-norm in general as $\boldsymbol{A} : \boldsymbol{A} = (\mathbf{a}^L)^{\mathrm{T}}\mathbf{a}^L = (\mathbf{a}^H)^{\mathrm{T}}\mathbf{a}^H$. The reason for that is, that both Lequeu's and Van Houtte's notations have an orthonormal basis of five symmetric second-order deviatoric tensors. Adding the normalized hydrostatic tensor completes the orthonormal basis $\{\boldsymbol{E}_i\}_{i=1,\dots,6}$ in the $\mathscr{R}^{3\times3}$ vector space, reading

$$\begin{aligned} \boldsymbol{E}_1 &= \frac{1}{\sqrt{3}}(\boldsymbol{e}_1\otimes\boldsymbol{e}_1 + \boldsymbol{e}_2\otimes\boldsymbol{e}_2 + \boldsymbol{e}_3\otimes\boldsymbol{e}_3) & \boldsymbol{E}_4 &= \frac{1}{\sqrt{2}}(\boldsymbol{e}_2\otimes\boldsymbol{e}_3 + \boldsymbol{e}_3\otimes\boldsymbol{e}_2) \\ \boldsymbol{E}_2 &= \frac{1}{\sqrt{6}}(-\boldsymbol{e}_1\otimes\boldsymbol{e}_1 - \boldsymbol{e}_2\otimes\boldsymbol{e}_2 + 2\boldsymbol{e}_3\otimes\boldsymbol{e}_3) & \boldsymbol{E}_5 &= \frac{1}{\sqrt{2}}(\boldsymbol{e}_1\otimes\boldsymbol{e}_3 + \boldsymbol{e}_3\otimes\boldsymbol{e}_1) \\ \boldsymbol{E}_3 &= \frac{1}{\sqrt{2}}(-\boldsymbol{e}_1\otimes\boldsymbol{e}_1 + \boldsymbol{e}_2\otimes\boldsymbol{e}_2) & \boldsymbol{E}_6 &= \frac{1}{\sqrt{2}}(\boldsymbol{e}_1\otimes\boldsymbol{e}_2 + \boldsymbol{e}_2\otimes\boldsymbol{e}_1) \end{aligned} \tag{15}$$

This basis is an alternative to the Mandel orthonormal basis, with the first three basis tensors related to the Mandel ones, as shown in Fig. 1. The tensor $\boldsymbol{E}_2$ is equal to the projected and normalized Mandel tensor $\boldsymbol{E}_2^M$ onto the π-plane, $\boldsymbol{E}_3$ lies in the π-plane and is orthonormal to $\boldsymbol{E}_2$, and $\boldsymbol{E}_1$ is normal to the π-plane. For the rest of the basis tensors, $\boldsymbol{E}_i = \boldsymbol{E}_i^M$ for $i = 4, 5, 6$.

Interestingly, the basis $\{\boldsymbol{E}_i\}$ carries tensor properties of crystals with cubic symmetry. Kocks et al. (1998) showed that the eigentensors of the elastic stiffness fourth-order tensor with cubic symmetry are the tensors belonging to the basis $\{\boldsymbol{E}_i\}$. Moreover, it can be shown that this basis also diagonalizes fourth-order compliance tensors of incompressible hexagonal crystals. Because of the uncoupling the deviatoric and the hydrostatic components, Kocks et al. (1998) denoted this basis as a

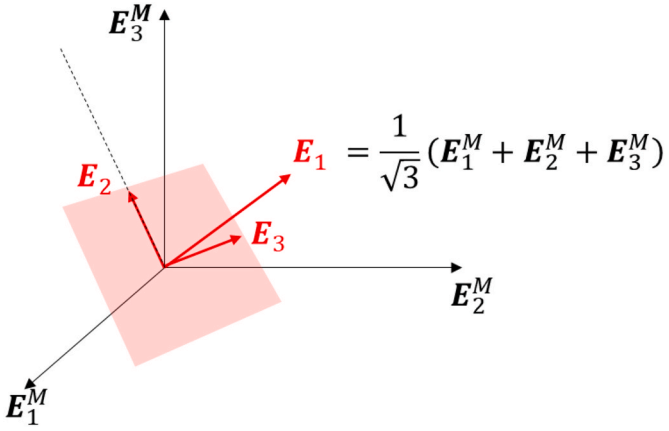

Fig. 1. Transformation of the Mandel basis.

natural basis. Consequently, in the following, the vector/matrix notation associated with the natural basis will be denoted as the natural notation.

A symmetric second order tensor $\boldsymbol{A}$ is expressed in the natural notation as $\boldsymbol{A} = a_i \boldsymbol{E}_i$, where

$$\mathbf{a} = \begin{pmatrix} a_1 \\ a_2 \\ a_3 \\ a_4 \\ a_5 \\ a_6 \end{pmatrix} = \begin{pmatrix} \frac{1}{\sqrt{3}}(A_{11}+A_{22}+A_{33}) \\ \frac{1}{\sqrt{6}}(2A_{33}-A_{11}-A_{22}) \\ \frac{1}{\sqrt{2}}(A_{22}-A_{11}) \\ \sqrt{2}\,A_{23} \\ \sqrt{2}\,A_{13} \\ \sqrt{2}\,A_{12} \end{pmatrix} \tag{16}$$

Note, that another orthonormal bases can be constructed by rotating basis tensors $\boldsymbol{E}_2$ and $\boldsymbol{E}_3$ around the $\boldsymbol{E}_1$ by an arbitrary angle θ (Fig. 1). The components of $\boldsymbol{A}$ then can be expressed as a function of angle θ as

$$\mathbf{a} = \begin{pmatrix} \frac{1}{\sqrt{3}}(A_{11}+A_{22}+A_{33}) \\ \frac{\sin\theta}{\sqrt{2}}(A_{11}-A_{22}) + \frac{\cos\theta}{\sqrt{6}}(2A_{33}-A_{11}-A_{22}) \\ \frac{\cos\theta}{\sqrt{2}}(A_{22}-A_{11}) + \frac{\sin\theta}{\sqrt{6}}(2A_{33}-A_{11}-A_{22}) \\ \sqrt{2}\,A_{23} \\ \sqrt{2}\,A_{13} \\ \sqrt{2}\,A_{12} \end{pmatrix} \tag{17}$$

For the case of a deviatoric tensor $\boldsymbol{A}'$ in which $A_{33} = -A_{11} - A_{22}$, the five deviatoric components in the natural notation degenerate in Lequeu and Van Houtte notations, for $\theta = -\frac{\pi}{2}$ and $\theta = -\frac{\pi}{12}$, respectively.

4. The natural notation applied to continuum elasto-plasticity

For modelling of plastic deformation in metals by the continuum plasticity theory, the classical assumption is that the plastic flow in metals is unaffected by the hydrostatic stress $p = \sigma_{ii}/3$. Pressure-independent yield functions, either isotropic or anisotropic, are typically employed when modelling plastic behavior of metals. Such a yield function is a function of the deviatoric stress, and so is the gradient, $\partial_{\boldsymbol{\sigma}} f$, and the Hessian, $\partial^2_{\boldsymbol{\sigma}\boldsymbol{\sigma}} f$. On the other hand, the hydrostatic stress is important when modelling plasticity of soil, clay, foams or any porous media, or for modelling of ductile fracture. Both, for computations involving pressure-dependent or independent plasticity calculations, it is beneficial to employ a vector/matrix notation, which not only takes advantage of the symmetry of the tensor but, in addition, explicitly contains the split of the deviatoric part and the spherical part in its components. In pressure-dependent models, the hydrostatic stress then does not need to be recomputed and becomes an explicit part of the notation. More importantly, in pressure-independent plasticity models, the yield function gradient and the Hessian are simplified, as the zero terms does not need to enter the computation. This directly results in dimension reduction of the linear or nonlinear systems to be solved. In the following, firstly transformation relations from the reference Voigt notation will be established. Those are further applied for expressing both elastic and plastic fourth-order tensorial properties in the natural notation. Eventually, application of the natural notation in an implicit backward Euler return-mapping algorithm is given in section 5.

4.1. Transformation relations with the Voigt notation

The natural basis uniquely defines the transformations matrices $\mathbf{T}_\sigma$ and $\mathbf{T}_\varepsilon$, which transform stress and strain written in Voigt notation to the natural notation, as

$$\boldsymbol{\sigma} = \mathbf{T}_\sigma \boldsymbol{\sigma}^V \quad \text{and} \quad \boldsymbol{\varepsilon} = \mathbf{T}_\varepsilon \boldsymbol{\varepsilon}^V, \tag{18}$$

where $\boldsymbol{\sigma}$ and $\boldsymbol{\varepsilon}$ are vector representations of stress and strain in the natural notation, respectively. These transformation tensors are related,

as $\mathbf{T}_\sigma = \mathbf{T}_\varepsilon^{-\mathrm{T}}$. The transformation matrices $\mathbf{T}_\sigma$, $\mathbf{T}_\varepsilon$, and their inverse $\mathbf{T}_\sigma^{-1}$, $\mathbf{T}_\varepsilon^{-1}$ read

$$
\begin{aligned}
\mathbf{T}_\sigma &= \frac{1}{\sqrt{6}}\begin{pmatrix} \sqrt{2} & \sqrt{2} & \sqrt{2} & 0 & 0 & 0 \\ -1 & -1 & 2 & 0 & 0 & 0 \\ -\sqrt{3} & \sqrt{3} & 0 & 0 & 0 & 0 \\ 0 & 0 & 0 & 2\sqrt{3} & 0 & 0 \\ 0 & 0 & 0 & 0 & 2\sqrt{3} & 0 \\ 0 & 0 & 0 & 0 & 0 & 2\sqrt{3} \end{pmatrix}, \\
\mathbf{T}_\varepsilon &= \frac{1}{\sqrt{6}}\begin{pmatrix} \sqrt{2} & \sqrt{2} & \sqrt{2} & 0 & 0 & 0 \\ -1 & -1 & 2 & 0 & 0 & 0 \\ -\sqrt{3} & \sqrt{3} & 0 & 0 & 0 & 0 \\ 0 & 0 & 0 & \sqrt{3} & 0 & 0 \\ 0 & 0 & 0 & 0 & \sqrt{3} & 0 \\ 0 & 0 & 0 & 0 & 0 & \sqrt{3} \end{pmatrix}, \\
\mathbf{T}_\sigma^{-1} &= \frac{1}{\sqrt{6}}\begin{pmatrix} \sqrt{2} & -1 & -\sqrt{3} & 0 & 0 & 0 \\ \sqrt{2} & -1 & \sqrt{3} & 0 & 0 & 0 \\ \sqrt{2} & 2 & 0 & 0 & 0 & 0 \\ 0 & 0 & 0 & \sqrt{3} & 0 & 0 \\ 0 & 0 & 0 & 0 & \sqrt{3} & 0 \\ 0 & 0 & 0 & 0 & 0 & \sqrt{3} \end{pmatrix}, \\
\mathbf{T}_\varepsilon^{-1} &= \frac{1}{\sqrt{6}}\begin{pmatrix} \sqrt{2} & -1 & -\sqrt{3} & 0 & 0 & 0 \\ \sqrt{2} & -1 & \sqrt{3} & 0 & 0 & 0 \\ \sqrt{2} & 2 & 0 & 0 & 0 & 0 \\ 0 & 0 & 0 & 2\sqrt{3} & 0 & 0 \\ 0 & 0 & 0 & 0 & 2\sqrt{3} & 0 \\ 0 & 0 & 0 & 0 & 0 & 2\sqrt{3} \end{pmatrix}
\end{aligned}
\tag{19}
$$

It is advantageous to formally write the volumetric part of $\mathbf{a}$ in Eq. (16) separately, as

$$
\mathbf{a} = \begin{pmatrix} \sqrt{3}\, a^{vol} \\ \mathbf{a}' \end{pmatrix} \tag{20}
$$

where $a^{vol} = \frac{1}{3}a_{ii}$ and $\mathbf{a}'$ denotes a 5-dimensional deviatoric vector with components given in Eq. (16). The volumetric part of a stress tensor, i.e. the hydrostatic stress, will be denoted as p.

4.2. Fourth-order elasticity tensors

A fourth-order tensor is written in the natural basis as $\mathbb{C} = C_{ij}\boldsymbol{E}_i \otimes \boldsymbol{E}_j$, where its coefficients C_{ij} can be written in a 6x6 matrix. The fourth-order tensors, e.g. elastic stiffness and compliance tensors, plastic anisotropy tensors etc., are originally in the literature expressed in the Voigt notation. Due to the distinction of contravariant and covariant Voigt bases, care must be taken when transforming a second or fourth-order tensor from Voigt to the natural (or also Mandel) notation. Since elasticity stiffness tensors are linear mappings of a strain (covariant) tensor to a stress (contravariant) tensor, it transforms as

$$
\mathbf{C} = \mathbf{T}_\sigma \mathbf{C}^V \mathbf{T}_\varepsilon^{-1}. \tag{21}
$$

An interesting consequence of using the natural notation, also pointed by Kocks et al. (1998), is that the elastic stiffness matrix for both isotropic and cubic symmetry transforms into a diagonal matrix as

$$
\begin{aligned}
\mathbf{C}^V_{\mathrm{iso}} &= \begin{pmatrix} 2\mu+\lambda & \lambda & \lambda & 0 & 0 & 0 \\ \lambda & 2\mu+\lambda & \lambda & 0 & 0 & 0 \\ \lambda & \lambda & 2\mu+\lambda & 0 & 0 & 0 \\ 0 & 0 & 0 & \mu & 0 & 0 \\ 0 & 0 & 0 & 0 & \mu & 0 \\ 0 & 0 & 0 & 0 & 0 & \mu \end{pmatrix} \\
\mathbf{C}_{\mathrm{iso}} &= \begin{pmatrix} 3K & 0 & 0 & 0 & 0 & 0 \\ 0 & 2\mu & 0 & 0 & 0 & 0 \\ 0 & 0 & 2\mu & 0 & 0 & 0 \\ 0 & 0 & 0 & 2\mu & 0 & 0 \\ 0 & 0 & 0 & 0 & 2\mu & 0 \\ 0 & 0 & 0 & 0 & 0 & 2\mu \end{pmatrix}
\end{aligned}
\tag{22}
$$

where λ is the Lamé's first parameter, μ the shear modulus and $K = \lambda + \frac{2}{3}\mu$ is the bulk modulus. For the case of cubic symmetry,

$$
\begin{aligned}
\mathbf{C}^V_{\mathrm{cub}} &= \begin{pmatrix} C_{11} & C_{12} & C_{12} & 0 & 0 & 0 \\ C_{12} & C_{11} & C_{12} & 0 & 0 & 0 \\ C_{12} & C_{12} & C_{11} & 0 & 0 & 0 \\ 0 & 0 & 0 & C_{44} & 0 & 0 \\ 0 & 0 & 0 & 0 & C_{44} & 0 \\ 0 & 0 & 0 & 0 & 0 & C_{44} \end{pmatrix} \\
\mathbf{C}_{\mathrm{cub}} &= \begin{pmatrix} C_{11}+2C_{12} & 0 & 0 & 0 & 0 & 0 \\ 0 & C_{11}-C_{12} & 0 & 0 & 0 & 0 \\ 0 & 0 & C_{11}-C_{12} & 0 & 0 & 0 \\ 0 & 0 & 0 & 2C_{44} & 0 & 0 \\ 0 & 0 & 0 & 0 & 2C_{44} & 0 \\ 0 & 0 & 0 & 0 & 0 & 2C_{44} \end{pmatrix}
\end{aligned}
\tag{23}
$$

This is practical for numerical computation, e.g. computing of the matrix inversion and for a matrix storage. Note, that $\mathbf{C}_{\mathrm{iso}}$ and $\mathbf{C}_{\mathrm{cub}}$ have the diagonal form for any angle θ in the general transformation Eq. (17). The elastic stiffness matrix with orthotropic symmetry in the natural notation is given in Appendix C.

4.3. The natural notation applied to quadratic yield functions

In the continuum plasticity computational codes, the most common isotropic yield function is the von Mises yield function. It can be expressed as a more general anisotropic quadratic yield function as

$$
\varphi(\boldsymbol{\sigma}) = \sqrt{\boldsymbol{\sigma} : \mathbb{M} : \boldsymbol{\sigma}} = \sqrt{(\boldsymbol{\sigma}^V)^{\mathrm{T}}\mathbf{M}^V\boldsymbol{\sigma}^V} = \sqrt{\boldsymbol{\sigma}^{\mathrm{T}}\mathbf{M}\,\boldsymbol{\sigma}} \tag{24}
$$

The fourth-order tensor $\mathbb{M}$ represents a linear mapping from a stress tensor to stress tensor. Its matrix in Voigt representation, $\mathbf{M}^V$, thus transforms into the natural notation according to

$$
\mathbf{M} = \mathbf{T}_\sigma^{-\mathrm{T}}\mathbf{M}^V\mathbf{T}_\sigma^{-1}, \tag{25}
$$

which results in

$$\mathbf{M}^V = \frac{1}{2}\begin{pmatrix} 2 & -1 & -1 & 0 & 0 & 0 \\ -1 & 2 & -1 & 0 & 0 & 0 \\ -1 & -1 & 2 & 0 & 0 & 0 \\ 0 & 0 & 0 & 6 & 0 & 0 \\ 0 & 0 & 0 & 0 & 6 & 0 \\ 0 & 0 & 0 & 0 & 0 & 6 \end{pmatrix}$$
$$\mathbf{M} = \frac{3}{2}\begin{pmatrix} 0 & 0 & 0 & 0 & 0 & 0 \\ 0 & 1 & 0 & 0 & 0 & 0 \\ 0 & 0 & 1 & 0 & 0 & 0 \\ 0 & 0 & 0 & 1 & 0 & 0 \\ 0 & 0 & 0 & 0 & 1 & 0 \\ 0 & 0 & 0 & 0 & 0 & 1 \end{pmatrix} \tag{26}$$

The diagonal form of $\mathbf{M}$ simplifies the expression of the von Mises criterion into $\varphi(\boldsymbol{\sigma}') = \sqrt{\frac{3}{2}\boldsymbol{\sigma}'^{\mathrm{T}}\boldsymbol{\sigma}'}$.

The Hill48 yield criterion (Hill, 1948) is the earliest version of an anisotropic criterion. It is a straightforward extension of the von Mises yield criterion and has a quadratic form. It is extensively used for modelling of plastic anisotropy in steels and is implemented in most of the commercial FE software. It has the same form as von Mises in Eq. (24), with the anisotropic matrix $\mathbf{M}$ in the Voigt and the natural notation as

$$\mathbf{M}^V = \begin{pmatrix} G+H & -H & -G & 0 & 0 & 0 \\ -H & F+H & -F & 0 & 0 & 0 \\ -G & -F & F+G & 0 & 0 & 0 \\ 0 & 0 & 0 & 2L & 0 & 0 \\ 0 & 0 & 0 & 0 & 2M & 0 \\ 0 & 0 & 0 & 0 & 0 & 2N \end{pmatrix}$$
$$\mathbf{M} = \frac{1}{2}\begin{pmatrix} 0 & 0 & 0 & 0 & 0 & 0 \\ 0 & 3(G+F) & \sqrt{3}(G-F) & 0 & 0 & 0 \\ 0 & \sqrt{3}(G-F) & F+G+4H & 0 & 0 & 0 \\ 0 & 0 & 0 & 2L & 0 & 0 \\ 0 & 0 & 0 & 0 & 2M & 0 \\ 0 & 0 & 0 & 0 & 0 & 2N \end{pmatrix} \tag{27}$$

The gradient, $\mathbf{g}'$, and Hessian, $\mathbf{H}'$, of the von Mises and Hill48 yield function are in the natural notation calculated as 5x1 and 5x5 matrix, respectively, reading

$$\mathbf{g}' = \frac{\mathbf{M}'\boldsymbol{\sigma}'}{\varphi}, \quad \mathbf{H}' = \frac{1}{\varphi}\left(\mathbf{M}' - \mathbf{g}'\mathbf{g}'^{\mathrm{T}}\right) \tag{28}$$

where $\mathbf{M}'$ denotes the deviatoric 5x5 submatrix of $\mathbf{M}$ (omitting first zeros-valued row and column).

4.4. The natural notation applied to linear transformation-based yield functions

Anisotropic yield functions based on the concept of linear transformation of the stress tensor, were first introduced by Sobotka (1969), Boehler and Sawczuk (1970). The concept was further generalized by Karafillis and Boyce (1993). The most recent examples of anisotropic yield functions constructed by linear transformation are Yld91 (Barlat et al., 1991), Yld2000-2d (Barlat et al., 2003), Yld2004-18p (Barlat et al., 2005) and more recent Yld2004-27p (Aretz et al., 2010), Yld2011-18p and Yld2011-27p (Aretz and Barlat, 2013). The main idea is the linear transformation of the Cauchy stress tensor as

$$\widehat{\boldsymbol{\sigma}} = \mathbb{L} : \boldsymbol{\sigma} \tag{29}$$

where $\widehat{\boldsymbol{\sigma}}$ is the transformed stress tensor and $\mathbb{L}$ is a fourth-order transformation tensor, representing the plastic anisotropy. Yld91 contains only one such transformation, whereas Yld2004-18p and Yld2011-18p are based on two transformations, by adding $\widehat{\widehat{\boldsymbol{\sigma}}} = \widehat{\widehat{\mathbb{L}}} : \boldsymbol{\sigma}$. Yld2004-27p and Yld2011-27p have three linear transformations, by including $\widehat{\widehat{\widehat{\boldsymbol{\sigma}}}} = \widehat{\widehat{\widehat{\mathbb{L}}}} : \boldsymbol{\sigma}$. Regardless of the number of transformations, the generic form (Eq. (29)) is in the literature expressed in the Voigt notation as

$$\widehat{\boldsymbol{\sigma}}^V = \mathbf{L}^V\boldsymbol{\sigma}^V = \mathbf{C}^V\mathbf{D}^V\boldsymbol{\sigma}^V \tag{30}$$

where $\mathbf{L}^V$ usually is decomposed into the anisotropic matrix $\mathbf{C}^V$ and the symmetric deviatoric projection matrix $\mathbf{D}^V$ that transforms the Cauchy stress $\boldsymbol{\sigma}^V$ to its deviator. The matrices $\mathbf{C}^V$ and $\mathbf{D}^V$ are

$$\mathbf{C}^V = \begin{pmatrix} 0 & -C_{12} & -C_{13} & 0 & 0 & 0 \\ -C_{21} & 0 & -C_{23} & 0 & 0 & 0 \\ -C_{31} & -C_{32} & 0 & 0 & 0 & 0 \\ 0 & 0 & 0 & C_{44} & 0 & 0 \\ 0 & 0 & 0 & 0 & C_{55} & 0 \\ 0 & 0 & 0 & 0 & 0 & C_{66} \end{pmatrix}$$
$$\mathbf{D}^V = \frac{1}{3}\begin{pmatrix} 2 & -1 & -1 & 0 & 0 & 0 \\ -1 & 2 & -1 & 0 & 0 & 0 \\ -1 & -1 & 2 & 0 & 0 & 0 \\ 0 & 0 & 0 & 3 & 0 & 0 \\ 0 & 0 & 0 & 0 & 3 & 0 \\ 0 & 0 & 0 & 0 & 0 & 3 \end{pmatrix} \tag{31}$$

The transformation of a stress vector in the natural notation is

$$\begin{pmatrix} \sqrt{3}\widehat{p} \\ \widehat{\boldsymbol{\sigma}}' \end{pmatrix} = \mathbf{L}\begin{pmatrix} \sqrt{3}p \\ \boldsymbol{\sigma}' \end{pmatrix} = \mathbf{CD}\begin{pmatrix} \sqrt{3}p \\ \boldsymbol{\sigma}' \end{pmatrix} \tag{32}$$

where $\mathbf{L}$ (and similarly $\mathbf{C}$ and $\mathbf{D}$) are obtained by the transformation

$$\mathbf{L} = \mathbf{T}_\sigma\mathbf{L}^V\mathbf{T}_\sigma^{-1}. \tag{33}$$

The properties of the natural notation make $\mathbf{D} = \mathbf{I}$, i.e. being equal to the identity matrix. Consequently,

$$\mathbf{L} = \mathbf{C} = \begin{pmatrix} 0 & L_{12} & L_{13} & 0 & 0 & 0 \\ 0 & L_{22} & L_{23} & 0 & 0 & 0 \\ 0 & L_{32} & L_{33} & 0 & 0 & 0 \\ 0 & 0 & 0 & L_{44} & 0 & 0 \\ 0 & 0 & 0 & 0 & L_{55} & 0 \\ 0 & 0 & 0 & 0 & 0 & L_{66} \end{pmatrix} \tag{34}$$

where

$$L_{12} = \frac{1}{3\sqrt{2}}(C_{12} - 2C_{13} + C_{21} - 2C_{23} + C_{31} + C_{32})$$
$$L_{13} = \frac{1}{\sqrt{6}}(-C_{12} + C_{21} + C_{31} - C_{32})$$
$$L_{22} = \frac{1}{6}(-C_{12} + 2C_{13} - C_{21} + 2C_{23} + 2C_{31} + 2C_{32})$$
$$L_{23} = \frac{1}{2\sqrt{3}}(C_{12} - C_{21} + 2C_{31} - 2C_{32})$$

$$L_{32} = \frac{1}{2\sqrt{3}}(-C_{12} + 2C_{13} + C_{21} - 2C_{23})$$
$$L_{33} = \frac{1}{2}(C_{12} + C_{21}) \tag{35}$$

and

$$L_{44} = C_{44}$$

$$L_{55} = C_{55}$$

$$L_{66} = C_{66}$$

Note that for the case of isotropic plasticity, $\mathbf{L}$ obtains a simple diagonal form in the natural notation, as

$$\mathbf{L}^{\text{iso}} = \begin{pmatrix} 0 & 0 & 0 & 0 & 0 & 0 \\ 0 & 1 & 0 & 0 & 0 & 0 \\ 0 & 0 & 1 & 0 & 0 & 0 \\ 0 & 0 & 0 & 1 & 0 & 0 \\ 0 & 0 & 0 & 0 & 1 & 0 \\ 0 & 0 & 0 & 0 & 0 & 1 \end{pmatrix} \tag{36}$$

In the definition of "YldXXX" yield functions, each linear transformation is defined by a matrix $\mathbf{L}$, which in general is not a deviatoric transformation, i.e. the transformed stress $\widehat{\boldsymbol{\sigma}}$ is usually not deviatoric. The exception is Yld91, which is constructed so that the transformed stress is deviatoric. This constraint reduces the number of independent coefficients in $\mathbf{L}$ from eight to six. The form of $\mathbf{L}$ in both Voigt and natural notation is similar to the Hill's anisotropy matrix (Eq. (27), as

$$\mathbf{L}^{V}_{\text{Yld91}} = \frac{1}{3}\begin{pmatrix} \overline{b}+\overline{c} & -\overline{c} & -\overline{b} & 0 & 0 & 0 \\ -\overline{c} & \overline{c}+\overline{a} & -\overline{a} & 0 & 0 & 0 \\ -\overline{b} & -\overline{a} & \overline{a}+\overline{b} & 0 & 0 & 0 \\ 0 & 0 & 0 & 3\overline{f} & 0 & 0 \\ 0 & 0 & 0 & 0 & 3\overline{g} & 0 \\ 0 & 0 & 0 & 0 & 0 & 3\overline{h} \end{pmatrix}$$
$$\mathbf{L}_{\text{Yld91}} = \frac{1}{6}\begin{pmatrix} 0 & 0 & 0 & 0 & 0 & 0 \\ 0 & 3\left(\overline{a}+\overline{b}\right) & \sqrt{3}\left(\overline{b}-\overline{a}\right) & 0 & 0 & 0 \\ 0 & \sqrt{3}\left(\overline{b}-\overline{a}\right) & \overline{a}+\overline{b}+4\overline{c} & 0 & 0 & 0 \\ 0 & 0 & 0 & 3\overline{f} & 0 & 0 \\ 0 & 0 & 0 & 0 & 3\overline{g} & 0 \\ 0 & 0 & 0 & 0 & 0 & 3\overline{h} \end{pmatrix} \tag{37}$$

All the linear transformation-based "YldXXX" yield functions are formulated as functions of the eigenvalues of the transformed stress tensors. Examples, with one and two linear transformations applied, are

$$\text{Yld91} = \varphi\left(\widehat{S}_1, \widehat{S}_2, \widehat{S}_3\right) = \left(\frac{1}{2}\left(\left|\widehat{S}_1 - \widehat{S}_2\right|^a + \left|\widehat{S}_2 - \widehat{S}_3\right|^a + \left|\widehat{S}_1 - \widehat{S}_3\right|^a\right)\right)^{\frac{1}{a}}$$

$$\text{Yld2004-18p} = \varphi\left(\widehat{S}_1, \widehat{S}_2, \widehat{S}_3, \widehat{\widehat{S}}_1, \widehat{\widehat{S}}_2, \widehat{\widehat{S}}_3\right) = \left(\frac{1}{4}\sum_{i,j=1}^{3}\left|\widehat{S}_i - \widehat{\widehat{S}}_j\right|^a\right)^{\frac{1}{a}}$$

$$\text{Yld2011-18p} = \varphi\left(\widehat{S}_1, \widehat{S}_2, \widehat{S}_3, \widehat{\widehat{S}}_1, \widehat{\widehat{S}}_2, \widehat{\widehat{S}}_3\right) = \left(\frac{1}{\xi}\sum_{i,j=1}^{3}\left|\widehat{S}_i + \widehat{\widehat{S}}_j\right|^a\right)^{\frac{1}{a}},$$
$$\xi = \left(\frac{4}{3}\right)^a + 4\left(\frac{2}{3}\right)^a + 4\left(\frac{1}{3}\right)^a \tag{38}$$

Recently, Cazacu (2019) derived explicit expressions of Yld91 for $a = 6$ and 8 in terms of the second and third invariants of the transformed deviatoric stress $\widehat{\boldsymbol{\sigma}}$. However, for yield functions involving two and three transformations, the eigenvalues of the transformed stress tensors need to be calculated. The analytical methods presented e.g. by Malvern (1969), Simo and Hughes (1998), Barlat et al. (2005), and later the robust method by Scherzinger and Dohrmann (2008), require calculation of the first, second and third invariant, I_1, I_2 and I_3 of the stress tensor. The analytical calculation of the gradient of Yld2004 given by Barlat et al. (2005) and Soare and Barlat (2011) requires the partial derivatives $\frac{\partial I_k}{\partial p}$ and $\frac{\partial I_k}{\partial \sigma_i}$ for $k = 1, 2, 3$ and $i = 1, \ldots, 5$. For the newly derived expressions for the Lankford coefficients of Yld91 (Cazacu, 2019), the derivatives $\frac{\partial J_k}{\partial p}$ and $\frac{\partial J_k}{\partial \sigma_i}$, for $k = 2, 3$ and $i = 1, \ldots, 5$ are needed, where J_2 and J_3 are the invariants of the deviatoric stress tensor. All calculated in the natural notation are given in Appendix A.

4.5. Orthogonal transformation in the natural notation

Assume $\boldsymbol{R}$ being an orthonormal transformation tensor which transforms the orthonormal basis $\{\boldsymbol{e}_i\}_{i=1,\ldots,3}$ into another orthonormal basis $\{\widehat{\boldsymbol{e}}_i\}_{i=1,\ldots,3}$ as $\widehat{\boldsymbol{e}}_i = \boldsymbol{R}^{\mathrm{T}} \cdot \boldsymbol{e}_i$. A second-order tensor $\boldsymbol{A}$ then transforms as $\widehat{\mathbf{A}} = \boldsymbol{R}^{\mathrm{T}} \cdot \boldsymbol{A} \cdot \boldsymbol{R}$ or in the indicial notation as $\widehat{A}_{kl} = R_{ik} R_{jl} A_{ij}$. A fourth-order tensor $\mathbb{C}$ transforms as $\widehat{C}_{mnop} = R_{im} R_{jn} R_{ko} R_{lp} C_{ijkl}$. In a reduced vector/matrix representation, a transformation of tensors $\boldsymbol{A}$ and $\mathbb{C}$ reads

$$\widehat{\mathbf{a}} = \mathbf{R}^{\mathrm{T}}\,\mathbf{a} \quad \text{and} \quad \widehat{\mathbf{C}} = \mathbf{R}^{\mathrm{T}}\,\mathbf{C}\,\mathbf{R} \tag{39}$$

The vectors $\mathbf{a}, \widehat{\mathbf{a}}$ and matrices $\mathbf{C}, \widehat{\mathbf{C}}$ are representations of tensors $\boldsymbol{A}$ and $\mathbb{C}$ in the given notation, before and after transformation, respectively. $\mathbf{R}$ and its transpose, $\mathbf{R}^{\mathrm{T}}$, are 6x6 matrices and represent the transformation in the given notation. In the Voigt notation, due to the its dual basis, the transformation matrix for transforming a stress-like tensor, $\mathbf{R}^{\mathrm{V}}_{\sigma}$, differs from the transformation matrix for a strain-like tensor, $\mathbf{R}^{\mathrm{V}}_{\varepsilon}$. Great care must be taken when transforming fourth-order tensors, as those can be of covariant, contravariant or of a mixed nature. This is avoided in both the Mandel and the natural notation which have one unique transformation matrix. The explicit forms of the 6x6 transformation matrix in the Voigt, Mandel and natural notation are given in Appendix B.

5. Application of the natural notation in a highly efficient and robust return-mapping algorithm

An extremely robust, implicit backward-Euler return-mapping algorithm with line-search was developed by Pérez-Foguet and Armero (2002). Recently, Scherzinger (2017) applied this algorithm to the non-quadratic, isotropic Hosford yield surface (Hosford, 1972) and to the anisotropic Yld2004-18p yield surface (Barlat et al., 2005). He showed excellent convergence, even for very large trial stress states. In addition, Scherzinger (2017) provided analytical expressions for the gradient and Hessian of the Hosford and of the Yld2004-18p yield surfaces. This algorithm with line-search is followed in this paper and further improved by applying the radial return as an initial guess for the Cauchy stress. Typically, return-mapping algorithms are in the literature formulated in their tensorial form, while numerical implementations employ either Voigt or Mandel vector/matrix notation. In the following, the return-mapping algorithm used by Scherzinger (2017) will be written directly in the natural notation.

The gradient and Hessian of a yield function, $\partial_{\boldsymbol{\sigma}} f$ and $\partial^2_{\boldsymbol{\sigma}\boldsymbol{\sigma}} f$, are second- and fourth-order tensors, respectively. In the numerical software they are typically computed and stored as a 6x1 vector, $\mathbf{g}^V$, and a 6x6 matrix, $\mathbf{H}^V$, respectively. As mentioned before, when written in the natural notation, because of the pressure-independence, the first component of $\mathbf{g}$ and the first row and column of $\mathbf{H}$ are zeros. Hence, only

the deviatoric non-zero 5x1 vector $\mathbf{g}'$ and 5x5 non-zero matrix $\mathbf{H}'$ are needed in the return-map. Using the transformation matrices given in Eq. (19), $\mathbf{g}^V$ and $\mathbf{H}^V$ can be transformed into the natural notation as

$$\mathbf{g} = \mathbf{T}_\sigma^{-\mathrm{T}} \mathbf{g}^V \quad \text{and} \quad \mathbf{H} = \mathbf{T}_\sigma^{-\mathrm{T}}\, \mathbf{H}^V\, \mathbf{T}_\sigma^{-1}. \tag{40}$$

Transformation of the Hessian in the explicit form is given in Appendix D. In the following, the implicit backward-Euler return-mapping algorithm with line-search (Pérez-Foguet and Armero, 2002; Scherzinger, 2017) will be given in the natural notation.

Given a strain increment $\Delta\boldsymbol{\varepsilon} = \begin{pmatrix} \sqrt{3}\Delta\varepsilon^{vol} & \Delta\boldsymbol{\varepsilon}' \end{pmatrix}^{\mathrm{T}}$ and the stress $\boldsymbol{\sigma}^{(n)} = \begin{pmatrix} \sqrt{3}p^{(n)} & \boldsymbol{\sigma}'^{(n)} \end{pmatrix}^{\mathrm{T}}$ at time t_n, the trial stress is obtained by applying the elastic predictor, as

$$\boldsymbol{\sigma}^{\mathrm{tr}} = \begin{pmatrix} \sqrt{3}p^{\mathrm{tr}} & \boldsymbol{\sigma}^{\mathrm{tr}'} \end{pmatrix}^{\mathrm{T}} = \boldsymbol{\sigma}^{(n)} + \mathbf{C}\Delta\boldsymbol{\varepsilon} \tag{41}$$

Note, that no plastic corrector is required for updating the hydrostatic part of the stress, i.e. $p^{\mathrm{tr}} = p^{(n+1)} = p^{(n)} + 3K\Delta\varepsilon^{vol}$. Thus, only the deviators $\boldsymbol{\sigma}^{\mathrm{tr}'}$, $\Delta\boldsymbol{\varepsilon}^{p'}$, $\mathbf{g}'$ and $\mathbf{H}'$ enter the plastic corrector part of the return-map, which was the aim for the new notation.

The plastic corrector part of the implicit backward-Euler return-map algorithm finds, in a iterative manner, the deviatoric stress $\boldsymbol{\sigma}'^{(n+1)}$ and the incremental plastic multiplier, $\Delta\gamma$, at time $t_{n+1} = t_n + \Delta t$, by solving the system of equations

$$\mathbf{r} = -\Delta\boldsymbol{\varepsilon}^{p'} + \Delta\gamma\, \mathbf{g}' = 0 \tag{42}$$

and

$$f = \varphi(\boldsymbol{\sigma}') - \sigma_Y = 0. \tag{43}$$

The plastic strain increment $\Delta\boldsymbol{\varepsilon}^{p'}$ is, due to the simple diagonal form of the isotropic elastic modulus in the natural notation (Eq. (22), a simple function of $\boldsymbol{\sigma}'$ as

$$\Delta\boldsymbol{\varepsilon}^{p'} = \frac{1}{2\mu}(\boldsymbol{\sigma}^{\mathrm{tr}'} - \boldsymbol{\sigma}'). \tag{44}$$

Iteratively, the stress $\boldsymbol{\sigma}'$ and the plastic multiplier $\Delta\gamma$ are updated as

$$\begin{aligned} \boldsymbol{\sigma}'^{(k+1)} &= \boldsymbol{\sigma}'^{(k)} + \Delta\boldsymbol{\sigma}' \\ \Delta\gamma^{(k+1)} &= \Delta\gamma^{(k)} + \Delta(\Delta\gamma) \end{aligned} \tag{45}$$

where (k) is the iteration, $\Delta\boldsymbol{\sigma}'$ and $\Delta(\Delta\gamma)$ are the increment of the deviatoric stress and the plastic multiplier, respectively.

Following Simo and Hughes (1998) or Scherzinger (2017), the Jacobian of the Newton-Raphson algorithm, a 5x5 matrix $\boldsymbol{\Xi}^{(k)}$, is needed for each iteration, in order to perform a Newton-Raphson increment. Its inverse, $\boldsymbol{\Xi}^{-1(k)}$ is calculated directly as

$$\boldsymbol{\Xi}^{-1(k)} = \frac{1}{2\mu}\mathbf{I} + \Delta\gamma^{(k)}\mathbf{H}'^{(k)} \tag{46}$$

A Newton-Raphson increment of $\Delta(\Delta\gamma)$ and the stress increment $\Delta\boldsymbol{\sigma}'$ are computed as

$$\begin{aligned} \Delta(\Delta\gamma) &= \frac{f^{(k)} - \mathbf{r}^{(k)\mathrm{T}}\, \boldsymbol{\Xi}^{(k)}\, \mathbf{g}'^{(k)}}{\mathbf{g}'^{(k)\mathrm{T}}\, \boldsymbol{\Xi}^{(k)}\, \mathbf{g}'^{(k)} + h^{(k)}} \\ \Delta\boldsymbol{\sigma}' &= -\boldsymbol{\Xi}^{(k)}\, \mathbf{r}^{(k)} - \Delta(\Delta\gamma)\, \boldsymbol{\Xi}^{(k)}\, \mathbf{g}'^{(k)} \end{aligned} \tag{47}$$

Here, $h^{(k)}$ is the plastic isotropic hardening modulus. However, the Jacobian $\boldsymbol{\Xi}^{(k)}$ itself does not need to be computed explicitly by rather expensive matrix inversion of $\boldsymbol{\Xi}^{-1(k)}$. Due to the symmetry of $\boldsymbol{\Xi}^{-1(k)}$, the effective Cholesky decomposition (Krishnamoorthy and Menon, 2013) can be applied to solve the linear systems

$$\begin{aligned} \boldsymbol{\Xi}^{-1(k)}\, \mathbf{x}_1 &= \mathbf{g}'^{(k)} \\ \boldsymbol{\Xi}^{-1(k)}\, \mathbf{x}_2 &= \mathbf{r}^{(k)} \end{aligned} \tag{48}$$

Having the solution vectors $\mathbf{x}_1$ and $\mathbf{x}_2$, Eq. (47) can be rewritten as

$$\begin{aligned} \Delta(\Delta\gamma) &= \frac{f^{(k)} - \mathbf{r}^{(k)\mathrm{T}}\mathbf{x}_1}{\mathbf{g}'^{(k)\mathrm{T}}\mathbf{x}_1 + h^{(k)}} \\ \Delta\boldsymbol{\sigma}' &= -\mathbf{x}_2 - \Delta(\Delta\gamma)\, \mathbf{x}_1 \end{aligned} \tag{49}$$

After each Newton-Raphson step, the convergence is measured by calculating a non-dimensional scalar residual function as

$$\psi^{(k)} = \frac{1}{2}\left(\mathbf{r}^{(k)\mathrm{T}}\mathbf{r}^{(k)} + \left(\frac{f^{(k)}}{2\mu}\right)^2 \right) \tag{50}$$

If for an iteration $(k+1)$, $\psi^{(k+1)} < \varepsilon$, then the algorithm has converged. If not, the $k+1$-th Newton-Raphson step is accepted only if the $\psi^{(k+1)}$ is lower than some fraction of $\psi^{(k)}$, which is the residual achieved in the previous Newton-Raphson iteration. Explicitly written, when

$$\psi^{(k+1)} < (1 - 2\beta)\psi^{(k)} \tag{51}$$

The parameter $\beta = 10^{-4}$, as recommended by Pérez-Foguet and Armero (2002).

If the condition in Eq. (51) is not satisfied, i.e. the Newton step is unfavorable, the updates for $\boldsymbol{\sigma}'^{(k+1)}$ and $\Delta\gamma^{(k+1)}$ in Eq. (45) are modified to an under-relaxed form as

$$\begin{aligned} \boldsymbol{\sigma}'^{(k+1)} &= \boldsymbol{\sigma}'^{(k)} + \alpha^{(k)}\Delta\boldsymbol{\sigma}' \\ \Delta\gamma^{(k+1)} &= \Delta\gamma^{(k)} + \alpha^{(k)}\Delta(\Delta\gamma) \end{aligned} \tag{52}$$

where $\alpha^{(k)}$ is a positive number less than 1 and controls the magnitude of the Newton-Raphson increments, $\Delta\boldsymbol{\sigma}'$ and $\Delta(\Delta\gamma)$. The value of $\alpha^{(k)}$ is found by a second iterative procedure, inside the Newton-Raphson (k)-th iteration, called the line-search, and reads

$$\alpha_{(j+1)}^{(k)} = \max\left(\eta\alpha_{(j)}^{(k)}, \frac{\left(\alpha_{(j)}^{(k)}\right)^2 \psi^{(k)}}{\psi_{(j)}^{(k+1)} - \left(1 - 2\alpha_{(j)}^{(k)}\right)\psi^{(k)}} \right). \tag{53}$$

The index (j) indicates iterations within the line search. The starting point is $\alpha_{(0)}^{(k)} = 1$. The parameter $\eta = 0.1$ (Pérez-Foguet and Armero, 2002; Scherzinger, 2017) controls the minimum value of $\alpha_{(j+1)}^{(k)}$. For each line search iteration (j), the merit function $\psi_{(j)}^{(k+1)}$ is calculated according to Eq. (50) using the updates of $\boldsymbol{\sigma}_{(j)}'^{(k+1)}$ and $\Delta\gamma_{(j)}^{(k+1)}$ calculated by using the step $\alpha_{(j)}^{(k)}$ as

$$\begin{aligned} \boldsymbol{\sigma}_{(j)}'^{(k+1)} &= \boldsymbol{\sigma}'^{(k)} + \alpha_{(j)}^{(k)}\Delta\boldsymbol{\sigma}' \\ \Delta\gamma_{(j)}^{(k+1)} &= \Delta\gamma^{(k)} + \alpha_{(j)}^{(k)}\Delta(\Delta\gamma) \end{aligned} \tag{54}$$

Within the line search iterations, the residual $\psi_{(j)}^{(k+1)}$ has to satisfy the Goldstein's condition (Goldstein, 1965; Pérez-Foguet and Armero, 2002).

$$\psi_{(j)}^{(k+1)} < \left(1 - 2\beta\alpha_{(j)}^{(k)}\right)\psi^{(k)} \tag{55}$$

If Eq. (55) is not satisfied, the line-search iterations continue by calculating new $\alpha_{(j+1)}^{(k)}$ using Eq. (53). On the other hand, if Eq. (55) is satisfied, then both the line search (j) and the Newton-Raphson (k) iteration are terminated by setting $\alpha^{(k)} = \alpha_{(j)}^{(k)}$, and performing the updates for $\boldsymbol{\sigma}'^{(k+1)}$ and $\Delta\gamma^{(k+1)}$ by Eq. (52). If the convergence is not reached, i.e. if $\psi^{(k+1)} \geq \varepsilon$, then the algorithm continues with next Newton-Raphson iteration.

Note, two mistakes have been introduced in the formulation of the return-map algorithm given by Scherzinger (2017), namely Eqs. (50) and (51), which in this paper are correctly written as Eqs. (53) and (55), respectively.

5.1. The radial-return initial guess – the radial-return predictor

In elastic predictor – plastic corrector type of return-mapping algorithms, the trial stress is normally considered as the initial guess, i.e. $\boldsymbol{\sigma}^{(0)} = \boldsymbol{\sigma}^{\mathrm{tr}}$, where $\boldsymbol{\sigma}^{\mathrm{tr}} = \boldsymbol{\sigma}^{(n)} + \mathbf{C}\,\Delta\boldsymbol{\varepsilon}$ is a result of the elastic predictor part. Correspondingly, $\Delta\gamma^{(0)} = 0$. The convergence can be improved when radial return of the trial stress onto the yield surface is used as the starting point for iterations. The initial guess for the stress, $\boldsymbol{\sigma}'(0)$ reads

$$\boldsymbol{\sigma}'(0) = \boldsymbol{\sigma}^{\mathrm{tr}'} \frac{\sigma_y}{\varphi(\boldsymbol{\sigma}^{\mathrm{tr}'})} \tag{56}$$

where σ_y is the yield stress.

The initial guess for the plastic multiplier increment, $\Delta\gamma$, is calculated accordingly as

$$\Delta\gamma^{(0)} = \frac{\Delta\boldsymbol{\varepsilon}^{p\prime\mathrm{T}}\boldsymbol{\sigma}'^{(0)}}{\sigma_y} = \frac{|\boldsymbol{\sigma}^{\mathrm{tr}'}|^2}{2\mu\varphi(\boldsymbol{\sigma}^{\mathrm{tr}'})}\left(1 - \frac{\sigma_y}{\varphi(\boldsymbol{\sigma}^{\mathrm{tr}'})}\right) \tag{57}$$

The initial guesses $\boldsymbol{\sigma}'(0)$ and $\Delta\gamma^{(0)}$ will be denoted the radial-return predictor.

Without any hardening, the initial guess, $\boldsymbol{\sigma}'(0)$, will lie on the yield surface, i.e. $f(\boldsymbol{\sigma}'(0)) = 0$. In the case of isotropic hardening, due to the non-zero initial $\Delta\gamma^{(0)}$, the yield surface will slightly expand and $\boldsymbol{\sigma}'(0)$ will be inside of the yield locus. As the consistency is not assured, at least one more Newton iteration is needed to find the solution. The initial guess can be improved for the case of von Mises yield surface with the isotropic hardening and calculated as

$$\boldsymbol{\sigma}'(0) = \boldsymbol{\sigma}^{\mathrm{tr}'}\left(1 - \frac{3\mu}{3\mu + h}\left(1 - \frac{\sigma_y}{\varphi(\boldsymbol{\sigma}^{\mathrm{tr}'})}\right)\right) \tag{58}$$

where h is the hardening modulus at the beginning of the time step. Such initial guess often satisfies the convergency criterion. Note, that for $h = 0$, Eq. (56) is recovered. For other yield functions than von Mises, the radial-return initial guess for stress given by Eq. (56) is to be used.

6. Results and discussion

6.1. Material models and model parameters

The implicit backward-Euler return-mapping algorithm described in Section 5, is implemented in a UMAT (user-defined material subroutine) for Abaqus/Standard 2020 and made freely available via GitLab repository (see Appendix). Isotropic elasticity was used. In the examples here, the Young's modulus E and Poisson's ratio ν are given in Table 1. Two plasticity models were implemented, the Hill48 and Yld2004-18p. For the implementation of the Yld2004-18p yield function, involving its gradient and Hessian, the recent analytical formulation by Scherzinger (2017) is followed but expressed in the natural notation. The robust solver by Scherzinger and Dohrmann (2008) was employed for computing eigenvalues and eigenvectors of symmetric 3x3 stress matrices.

In order to compare the performance of Yld2004-18p to Hill48, anisotropy coefficients of the Yld2004-18p were chosen so that Yld2004-18p reduces into Yld91 (Barlat et al., 1991, 2005), since Yld91 further coincides with Hill48, for an exponent $a = 2$, as shown in the Appendix of Barlat et al. (2007). The explicit link between the six Hill48 coefficients and the six independent Yld2004-18p coefficients are given in Appendix E.

The isotropic hardening is provided by the Voce law as

$$R = R_{sat}\left(1 - \exp\left(-\frac{\bar{\varepsilon}}{\Delta\varepsilon_{sat}}\right)\right) \tag{59}$$

with the analytical hardening modulus

$$h = \frac{\mathrm{d}R}{\mathrm{d}\bar{\varepsilon}} = \frac{R_{sat} - R}{\Delta\varepsilon_{sat}} \tag{60}$$

The saturation stress R_{sat} and the strain scale $\Delta\varepsilon_{sat}$ as well as the initial yield stress σ_y, are given in Table 1. For the chosen values, the uniform strain is approximately 0.5.

6.2. Performance of the return-mapping algorithm implemented in the natural and Voigt notation

In both pressure-dependent and pressure-independent plasticity models, the constitutive equations require a split of a stress and strain-rate tensor into deviatoric and volumetric parts. Since the natural notation inherently contains the deviatoric and volumetric part of the tensor, it is beneficial to use it for formulating the constitutive relations, as well as the numerical algorithm for solving them. As shown in section 4, utilization of the natural notation is advantageous when expressing both elastic as well as plastic tensorial quantities, as this leads to more concise expressions. Examples are the diagonalization of isotropic as well as cubic-symmetry elastic moduli, and the reduction from six to five dimensions for both the gradient and Hessian of a yield function, further resulting in the reduced system of equations to solve in a fully implicit return-mapping algorithm.

In this section, the computational performance of the backward Euler return-mapping algorithm implemented in the natural and Voigt notation, described in section 5, is tested. For this, 10 000 uniformly distributed strain increments were used in the return-mapping algorithm, and one time step was computed for each, using $\Delta t = 0.01$. Both Hill48 and Yld2004-18p yield functions were tested, with parameters given in Table 1. For Yld2004-18p, exponents of 2, 4, 6, 8, 12 and 20 were used in this comparison. The relative reduction in the computational time when using the natural notation, as compared to the Voigt notation, is shown in Fig. 2. The largest relative speedup is achieved for the Hill48 yield function, $\sim 23\%$, while this reduces down to $\sim 5\%$ for Yld2004-18p. The part of the algorithm with the highest relative computational time reduction is the linear system solver by Cholesky

Table 1
Material parameters. The anisotropic C-coefficients are related to Yld2004-18p yield surface and Eq. (31), the coefficients F, G, H, L, M and N are related to Hill48 yield surface and Eq. (27).

E		ν		σ_y		R_{sat}		$\Delta\varepsilon_{sat}$
70 GPa		0.3		20 MPa		150 MPa		0.5
C_{12}	C_{13}	C_{21}	C_{23}	C_{31}	C_{32}	C_{44}	C_{55}	C_{66}
0.813	0.880	0.658	0.578	0.808	0.653	0.922	0.637	0.901
F	G	H	L	M	N			
0.105	0.446	0.281	1.275	0.609	1.218			

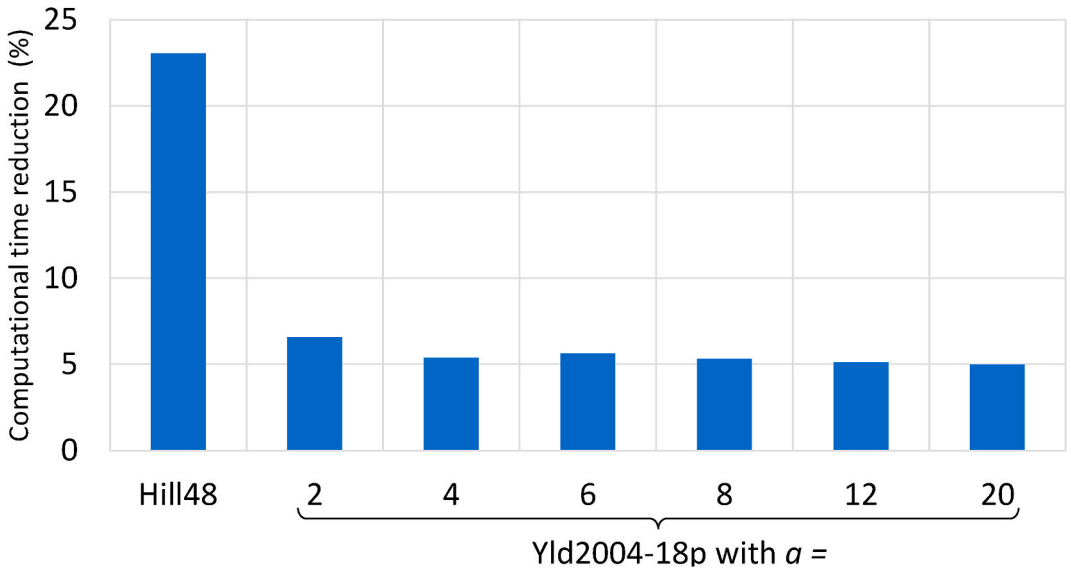

Fig. 2. Relative computational time reduction for the implementation of the return-mapping algorithm in the natural notation as compared to the Voigt notation implementation. Yld2004-18p yield function with exponent a between 2 and 20 was tested.

decomposition, which needs about ∼ 60% less time to solve a 5-dimensional system as compared to 6-dimensions. Other time-saving parts are the construction of and manipulation with the Hessian and elastic modulus, as both implicitly contain more zero components in the natural notation as compared to the Voigt notation. However, these time reducing parts of the algorithm play a smaller role for the case of Yld2004-18p than for Hill48, as the computation of Yld2004-18p, its gradient and the Hessian are computationally more complex.

6.3. *Effect of the radial return initial guess*

In a predictor-corrector return-mapping algorithm, trial stress obtained by the elastic predictor given in Eq. (41) is normally used as the initial guess for stress in the plastic corrector iteration process. The plastic multiplicator increment, $\Delta\gamma$, is initially equal to 0. However, for a large time step, the trial stress lies relatively far from the yield surface. Some Newton iterations need to be spent to bring it onto the yield surface. Alternatively, a radial projection of the trial stress directly on the yield surface can be calculated according to Eq. (56), and such a radially returned stress can instead serve as the initial guess.

In order to test the effect of the radial return initial guess, 200 000 trial stress states, evenly distributed outside of the yield surface with effective stress magnitudes up to 40 times the yield stress, were chosen. This is a large set that effectively covers the range of trial stress states that can be seen in a numerical simulation. The material parameters applied are given in Table 1. Note, that the use of an even distribution of trial stress states in the 5-dimensional deviatoric stress space makes the convergence statistics very little dependent on the choice of the specific anisotropy coefficients applied in the test. The exponents of Yld2004-18p that was tested were 6, 8, 12, 20 and 100.

Fig. 3 shows convergence statistics for cases with the trial stress as the initial guess (top row) and for cases with the radial return initial guess (bottom row). Statistical distributions, based on the 200 000 stress states tested, are made for the number of Newton-iterations and for the

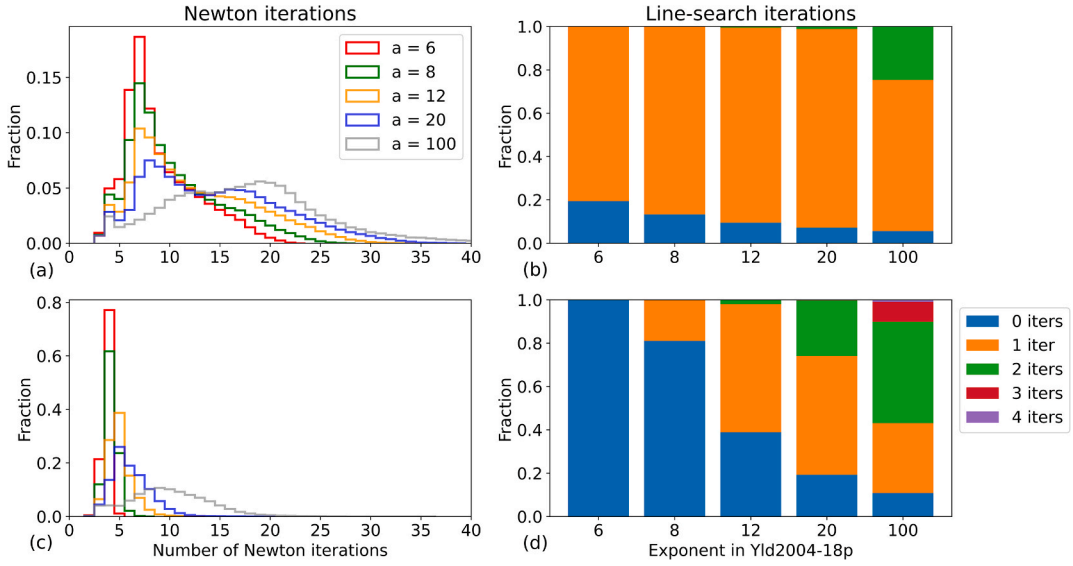

Fig. 3. Distributions of the number of Newton iterations (a), (c) and line-search iterations (b), (d) until the convergence as a function of the exponent a in Yld2004-18p. Subplots in the upper row represent cases with trial stress used as a starting point, the lower row applies for cases with radial return initial guess. Results are based on 200 000 trial stress states evenly distributed outside of the yield surface with effective stress magnitudes up to 40 times the yield stress.

number of line-search iterations. The radial return initial guess greatly reduces the number of Newton iterations for all the exponents tested. When the elastic predictor is used, the largest number of iterations recorded was 55 for the case with an exponent of 100 (out of the plotted range in Fig. 3a). For the exponent 6, which is an important case for modelling of BCC metals, some trial stress states may need up to 23 N iterations to converge. By using the radial return initial guess, none of the stress states requires more than 5 N iterations. In addition, the line-search part of the algorithm was not required. For an exponent 8, i.e. the important case relevant for FCC metals, the number of Newton iterations for the slowest converging case is 28. However, this drops down to 8 applying the radial return guess, and the number of cases that needs to activate a line-search is greatly reduced.

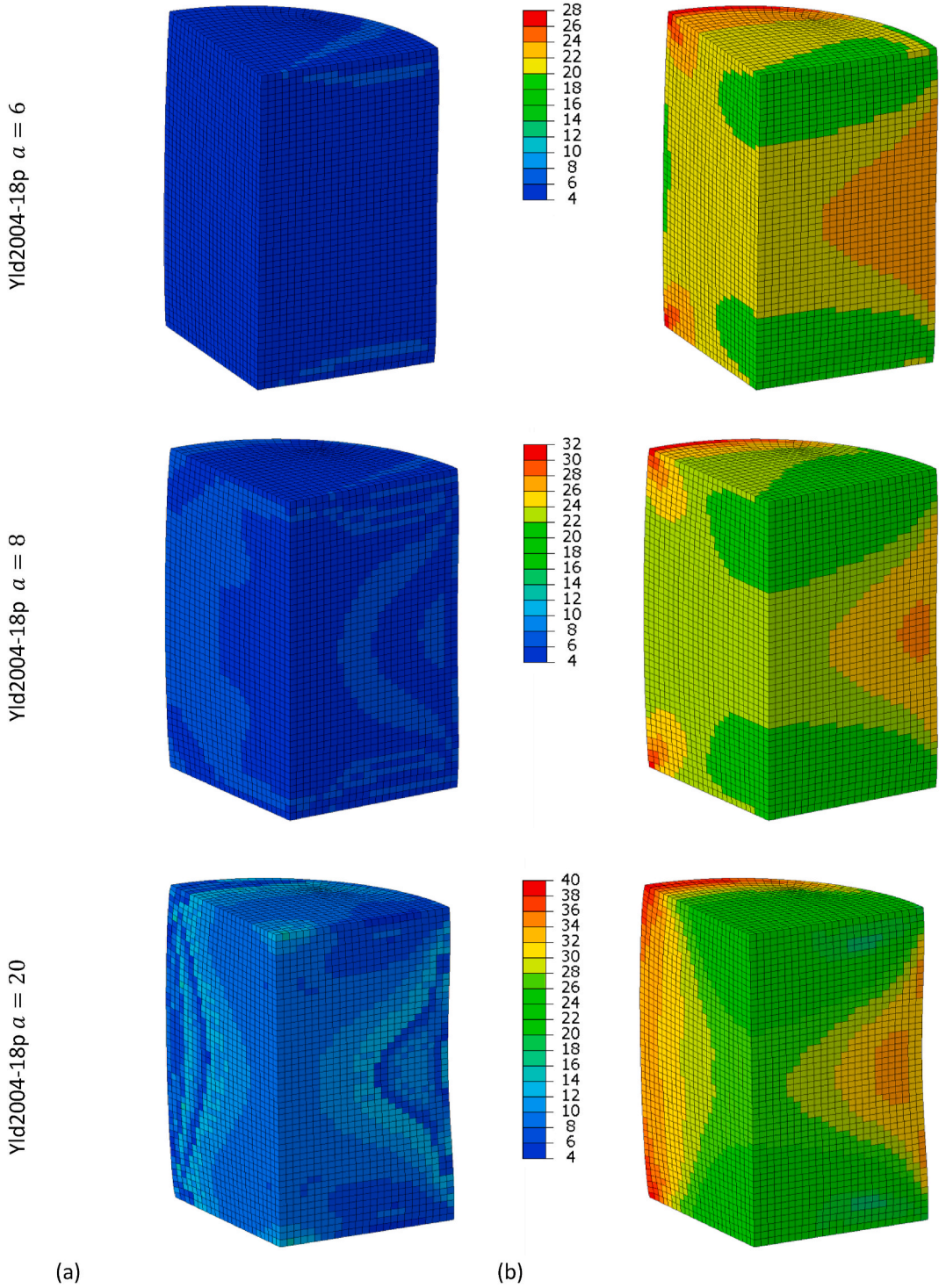

Fig. 4. Number of Newton iterations needed for the return-mapping algorithm to converge when (a) using the radial return initial guess and (b) using the trial stress state as the initial guess. Yld2004-18p yield function with parameters given in Table 1 and exponents of 6, 8 and 20 was used. Results are taken at approximately 15% of compression.

6.4. FE simulation of a compression test of a bulk cylinder

A uniaxial compression of a cylindrical bar was simulated by Abaqus/Standard 2020, using the implicit direct FE solver. Both the height and diameter of the bar were 100 mm. Only one quarter of the bar was modelled, due to orthotropic symmetry of both Hill48 and Yld2004-18p. The bar geometry was meshed by ∼30 000 elements of type C3D8R. A 25% high reduction by uniaxial compression was performed by a rigid tool with a Coulomb friction of 0.1 between the tool and the bar. The model parameters applied are listed in Table 1. The anisotropy x-axis coincides with the compression direction.

Results of FE simulations at ∼ 15% compression are shown in Fig. 4. The number of Newton iterations needed for the return-mapping algorithm to converge is presented for each element. Examples with exponents 6,8 and 20 of the Yld2004-18p are shown. When the radial return initial guess was used, 8 N iterations at most were needed for exponents 6 and 8, while at least 15 and as many as 32 iterations were spent for the return-map to converge when the trial stress was used as the initial guess. The results with an exponent equal 20 show somewhat clearer an onset of localization, i.e. barreling, which is promoted by a more faceted Tresca-like yield surface with sharper corners than with exponents 6 and 8. The localization region involve sharper strain-path changes, which normally requires an increased number of iterations by the return-map.

6.5. FE simulation of a uniaxial tension

A quasi-static FE simulation of a uniaxial tension of a flat specimen was performed. The thickness of the sample is 3 mm, the length and width of the gauge area is 50 mm and 15 mm, respectively. The tensile specimen was meshed by ∼17 000 elements of type C3D8R. The model parameters used were the same as for the compression case, given in Table 1. The anisotropy x-axis coincides with the tensile direction.

Results of FE simulations at ∼ 25% plastic strain for different initial guess at the beginning of the return-mapping algorithm are shown in Fig. 6. The number of Newton iterations needed for the return-mapping algorithm to converge, is presented for each element. Examples with exponents 6, 8 and 20 of the Yld2004-18p are shown. When the radial return initial guess was used, 4 N iterations were needed for exponents 6 and 8, while up to 16 iterations were needed when the trial stress was used as the initial guess.

The chosen initial yield stress and the isotropic hardening allow the material to harden until the uniform strain, which is ∼ 50%. During the FE simulation, a stable return-mapping algorithm allows Abaqus to automatically increase the time increment during the simulation. The time increment as well as the strain increment enter the UMAT as an input. As an example, Fig. 5 shows the total equivalent strain together with the equivalent strain increments per time step during the FE simulation of a uniaxial tension, using Yld2004-18p with an exponent of 6. As the material hardens, the equivalent strain increment increases and reaches ∼0.075. For the given Young's modulus, the elastic predictor results in trial stress above 5 GPa, which for the equivalent stress of ∼100 MPa makes the yield function 50 times larger than the equivalent stress. Using the radial return predictor instead of the elastic predictor, avoids the large jump of the stress into the plastic region and hence improves the convergence of the return-mapping algorithm. However, a more effective return-mapping algorithm will not affect the global convergence behavior of the FE solver.

6.6. FE simulation of a compression of a thin-walled tube

Compression of a thin-walled tube was run in an implicit quasi-static FE simulation with contact. The dimensions of the tube were 200 mm (height) x 100 mm (width) x 100 mm (length), and the wall thickness was 4 mm. A Coulomb friction coefficient of 0.1 was used for the friction between the rigid circular plates and the tube. Plastic buckling of the tube occurred early after the beginning of the test. The FE model consisted of ∼44 000 solid elements with reduced integration (type C3D8R) and hourglass control. The model parameters, except for the isotropic hardening, were the same as for the previous analyses. The isotropic hardening for this case was chosen to reflect a T6 condition for an AA6082 aluminium alloys, which has typically little work hardening potential and a uniform strain below 0.1. The Voce law as in Eq. (59), was applied with parameters $R^{sat} = 40$ MPa, $\Delta\varepsilon^{sat} = 0.05$. The initial yield stress was 300 MPa. The anisotropy x-axis coincides with the compression direction.

Results of FE simulations at 18% global strain, obtained using the Yld2004-18p yield criterion with exponent 8, are shown in Fig. 7, for both radial-return and elastic predictor. The number of Newton iterations needed for the return-mapping algorithm to converge, is presented by the color code for each element. In this case, the average number of iterations is much smaller as compared to the bulk cylinder compression in Section 6.4. This is due to smaller time steps chosen by Abaqus in the current simulation. Hence, for lower trial stresses, the gain by applying the radial return predictor is smaller.

6.7. Overall performance of the FE simulations with UMAT, using the new return-mapping algorithm

The performance of the new return-mapping algorithm was tested by running FE simulations of uniaxial tension and compression of both bulk cylinder and thin-walled tube. The quadratic von Mises and Hill48 yield criteria and the Yld2004-18p yield criterion with various yield-surface exponents were tested. The total time of each simulation was recorded. All simulations were run by Abaqus/Standard 2020 using the direct solver on a Windows 10 system on Intel Core i7-7700 CPU 3.6 GHz. The simulations of the uniaxial tensile test and the compression test of a cylinder were run on a single cpu without any parallelization. The tube compression was run on four cpus. Automatic time incrementation was

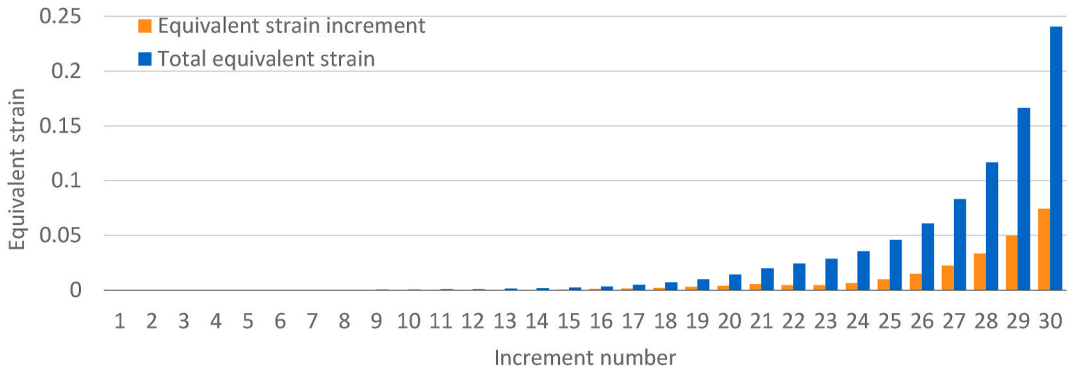

Fig. 5. Equivalent strain and strain increment during increment in a FE simulation of uniaxial tensile test by implicit FE solver Abaqus/Standard using Yld2004-18p yield function with exponent of 6 and material parameters from Table 1.

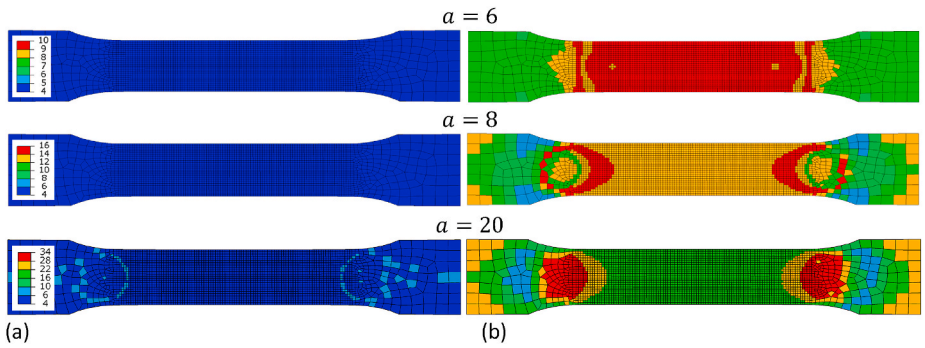

Fig. 6. Number of Newton iterations needed for the return-mapping algorithm to converge, when (a) using the radial return initial guess, and (b) using the trial stress state as the initial guess. The Yld2004-18p yield function with parameters given in Table 1 and exponents $a = 6$, 8 and 20 was used. Results are taken at approximately 30% deformation.

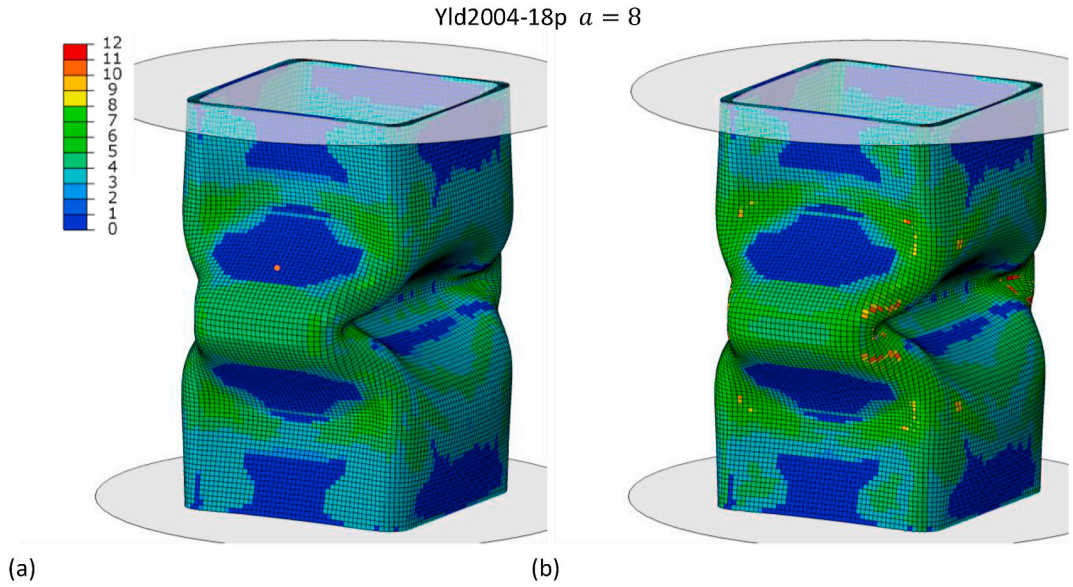

Fig. 7. Number of Newton iterations needed for the return-mapping algorithm to converge, when (a) using the radial return initial guess, and (b) using the trial stress state as the initial guess. The Yld2004-18p yield function with parameters given in Table 1 and exponent of 8 was used. Results are taken at 18% of compression.

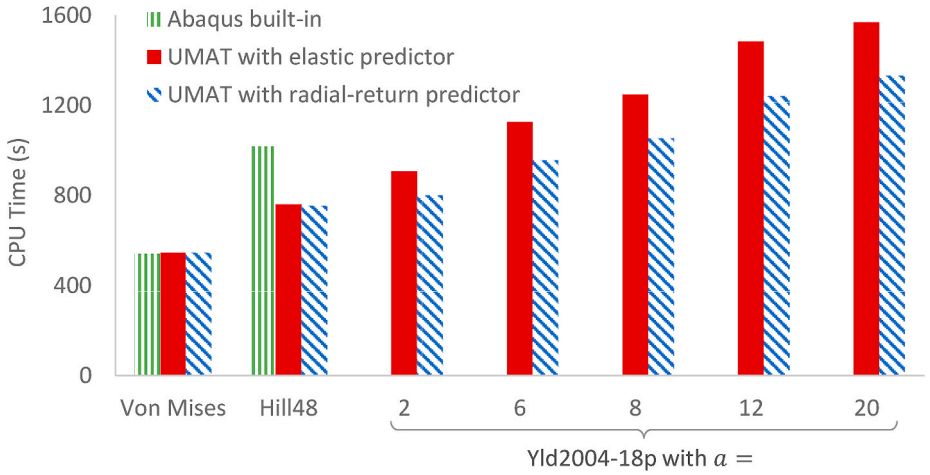

Fig. 8. Comparison of the overall computational performance of FE simulations of the uniaxial compression using von Mises, Hill48 and Yld2004-18p yield functions. The effect of elastic predictor and radial return predictor in the return-mapping algorithm are compared. Simulations were run up to a compression strain of 25%.

chosen, so that Abaqus could increase the time increments when global convergence was easy to achieve. As shown earlier, the new return-mapping algorithm will efficiently provide well-converged solution of the material model in a robust manner. On the other hand, when global convergence is difficult to establish, Abaqus applies cutbacks and reduces the time increment to reach convergence. An initial time increment of 0.01 was chosen, and the total time was 1.

As mentioned earlier, the anisotropy parameters of Yld2004-18p and Hill48 are related by Eq. (78), so that the model using Yld2004-18p with exponent $a = 2$ is equivalent to the model employing the Hill48 yield criterion.

Timing results of the FE simulations of three tests, i.e. the compression of a bulk cylinder, the uniaxial tension of a flat specimen and the compression of a thin-walled tube, are presented in Fig. 8, Fig. 9 and Fig. 10, respectively. For benchmarking purposes, the Abaqus' built-in von Mises and Hill48 plasticity models were run (vertical-stripe patterned bars). Results of the first two tests show improvement in the performance, when the radial-return predictor is used together with the Yld2004-18p model. This is due to relatively large time steps during the FE analysis. It is found for the cases tested, that with the largest exponents, the effect of the radial-return predictor is strongest. In the thin-walled tube compression test, significant plastic buckling takes place, which causes reduction of the time steps. Smaller time steps result in smaller trial stresses, and the gain by applying the radial-return predictor is limited for this case.

Fig. 9 shows that the Hill48 model in UMAT ran slightly faster than the von Mises model in UMAT for the uniaxial tension. However, it must be noted that the von Mises model in UMAT here is computed as a special case of Yld2004-18p, which is more complex than computing Hill48. On the other hand, the von Mises model reaches convergence directly by the radial-return predictor, while the Hill48 model typically needs up to 4 iterations to converge.

The von Mises model ran from UMAT, performs very close to the Abaqus' built-in von Mises model. This is expected, as the radial return direction is actually equal to the Euler backward direction. For all three tests, the Hill48 model from UMAT performed better than the Abaqus' built-in Hill48 model, regardless of the predictor type used. For the case of bulk compression, the difference is surprisingly large. More time step cutbacks were needed in order to achieve the convergence. The less stable behavior of the Abaqus' built-in Hill48 model was not observed when running any of the new models in UMAT.

Perhaps the most important result from Figs. 8, Figs. 9 and 10, is that the overall computational performance for models employing Yld2004-18p with $a = 6$ and 8 are comparable to the simplest von Mises or Hill48 models. In all three tests, using the radial-return predictor, the performance of Yld2004-18p with exponent up to 8 matches the performance of the built-in Hill48 Abaqus model within 20%. Note that the stability and efficiency of the algorithm enable the Yld2004-18p yield function for use in FE simulations. Note also, the comparable performance of an implicit FE simulation when using Yld2004-18p and Hill48 model, makes the Yld2004-18p eligible to become a natural part of any commercial FE software package suited for nonlinear structural mechanics of continua.

The relatively high number of anisotropy coefficients to be calibrated (16 independent ones, as proved by van den Boogaard et al. (2016)) can in simplified applications be reduced to the same number as for Hill48 (Yld2004-18p reduces to Yld91), so that standard mechanical testing procedures, already established, for identification of the Hill48's coefficients, can be applied also for high-exponent yield criteria. The possibility to adjust the yield-surface exponent to reflect the crystallography of the metal tested, comes at a very small extra cost.

On the other hand, the number of adjustable parameters can also be further extended, as in Yld2004-27p (Aretz et al., 2010) or Yld2011-27p (Aretz and Barlat, 2013), which might be necessary for the concept of a "virtual testing laboratory", in which no restrictions exist on the type and number of mechanical tests applicable to determine these parameters.

7. Conclusions

A natural notation has been introduced, which is adequate for formulations and implementations of continuum plasticity models. Applying this formalism, efficient and robust implicit backward Euler return-mapping algorithm with radial return predictor was implemented. Due to the explicit representation of a deviatoric and volumetric part, the natural notation was shown to be advantageous for expressing symmetric second- and fourth-order tensors in continuum plasticity. Its application in a return-mapping algorithm for pressure-independent yield functions led to dimensionality reduction of the system of equations to be solved. The natural notation lowered the computational cost of the return-mapping algorithm compared to the traditional Voigt notation, for Hill48 plasticity model by almost 25%.

The elastic predictor in the return-mapping algorithm was replaced by the radial return predictor, which uses radial projection of the trial stress onto the yield surface as the initial guess. This starting guess considerably improved the convergence of the return-map, particularly for large strain increments.

The presented return-mapping algorithm was implemented for Hill48 and Yld2004-18p yield functions in the user-defined material subroutine (UMAT) for Abaqus/Standard. FE simulations of a uniaxial

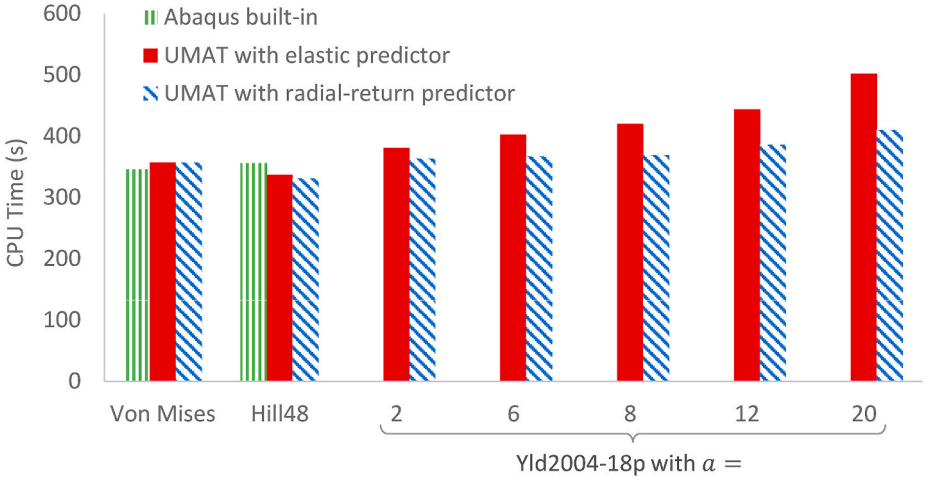

Fig. 9. Comparison of the overall computational performance of FE simulation of the uniaxial tension using von Mises, Hill48 and Yld2004-18p yield functions. The effect of elastic predictor and radial return predictor in the return-mapping algorithm are compared. Simulations were run up to an equivalent strain of ∼50%.

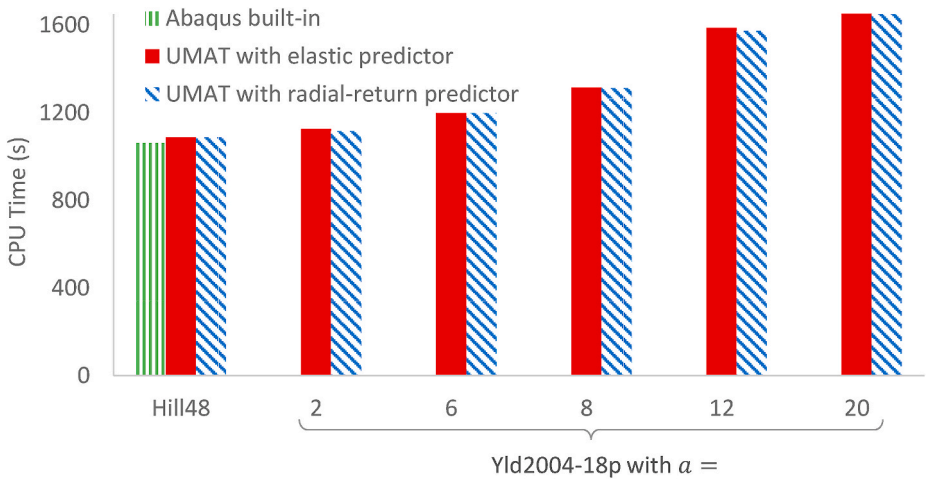

Fig. 10. Comparison of the overall computational performance of FE simulation of the compression of a thin-walled tube using von Mises, Hill48 and Yld2004-18p yield functions. The effect of elastic predictor and radial return predictor in the return-mapping algorithm are compared. Simulations were run up to a global compression of 18%.

tension test and a uniaxial compression test with contact were run, testing several exponents up to 20 of Yld2004-18p. The main conclusion is that for some cases the overall computational cost of simulations employing Yld2004-18p is comparable to the simplest von Mises and Hill48 models. When contact is involved and causing reduction of the time increment, the higher cost of the more complex Yld2004-18p becomes more dominant.

The results show that the new return-mapping algorithm employing Yld2004-18p is equally fast and robust as the simple von Mises and Hill implementations in the Abaqus/Standard software. This demonstrates the competitiveness of Yld2004-18p for applications using implicit FE simulations. By now, only very few commercial FE software contain the Yld2004-18p as the built-in material model. The author hopes that the presented return-mapping algorithm and the provided numerical implementation enable the full exploitation of advanced yield functions in industrial FE software. This will lower the threshold for their use and may set the new standard for the metal forming industry.

Credit author statement

Tomas Manik: Conceptualization, Methodology, Software, Validation, Formal analysis, Visualization, Writing – original draft preparation

Funding

This research did not receive any specific grant from funding agencies in the public, commercial, or not-for-profit sectors.

Declaration of competing interest

The authors declare that they have no known competing financial interests or personal relationships that could have appeared to influence the work reported in this paper.

Acknowledgements

I wish to express my gratitude to Prof. Bjørn Holmedal for discussions initiating the present paper and for helpful comments. This work received support from the METPLAST project, FRIPRO grant 315727, Research Council of Norway.

Appendix

The UMAT developed in this work can be freely downloaded from the following link:
https://gitlab.com/ntnu-physmet/continuum-plasticity

A. *Stress Invariants and their derivatives in the natural notation*

Using the natural notation of a stress tensor $\boldsymbol{\sigma}$ in the form given by Eq. (20) as $\boldsymbol{\sigma} = (\sqrt{3}p \quad \boldsymbol{\sigma}')^{\mathrm{T}}$, where $\boldsymbol{\sigma}' = (\sigma'_1, \sigma'_2, \sigma'_3, \sigma'_4, \sigma'_5)^{\mathrm{T}}$, the invariants I_1, I_2, I_3 of $\boldsymbol{\sigma}$ as well as the invariants J_1, J_2, J_3 of the deviator $\boldsymbol{\sigma}'$ are calculated as

$$
\begin{aligned}
I_1 &= \mathrm{tr}(\boldsymbol{\sigma}) = p \\
I_2 &= \frac{1}{2}\left(\mathrm{tr}(\boldsymbol{\sigma}^2) - \mathrm{tr}(\boldsymbol{\sigma})^2\right) = \frac{1}{2}\boldsymbol{\sigma}'^{\mathrm{T}}\,\boldsymbol{\sigma}' - 3p^2 \\
I_3 &= \det(\boldsymbol{\sigma}) = \frac{1}{\sqrt{2}}\sigma_3'\sigma_4'\sigma_5' \\
&\quad -\frac{1}{2\sqrt{6}}\sigma_3'^{\,2}\left(\sqrt{2}\,p - \sigma_1' - \sqrt{3}\,\sigma_2'\right) - \frac{1}{2\sqrt{6}}\sigma_4'^{\,2}\left(\sqrt{2}\,p - \sigma_1' + \sqrt{3}\,\sigma_2'\right) - \frac{1}{2\sqrt{6}}\sigma_5'^{\,2}\left(\sqrt{2}\,p + 2\sigma_1'\right) \\
&\quad +\frac{1}{6\sqrt{6}}\left(\sqrt{2}\,p - \sigma_1' - \sqrt{3}\,\sigma_2'\right)\left(\sqrt{2}\,p - \sigma_1' + \sqrt{3}\,\sigma_2'\right)\left(\sqrt{2}\,p + 2\sigma_1'\right) \\
J_1 &= \mathrm{tr}(\boldsymbol{\sigma}') = 0 \\
J_2 &= \frac{1}{2}\mathrm{tr}(\boldsymbol{\sigma}'^2) = \frac{1}{2}\boldsymbol{\sigma}'^{\mathrm{T}}\,\boldsymbol{\sigma}' \\
J_3 &= \det(\boldsymbol{\sigma}') = \frac{1}{\sqrt{2}}\sigma_3'\sigma_4'\sigma_5' + \frac{1}{2\sqrt{6}}\sigma_3'^{\,2}\left(\sigma_1' + \sqrt{3}\,\sigma_2'\right) \\
&\quad +\frac{1}{2\sqrt{6}}\sigma_4'^{\,2}\left(\sigma_1' - \sqrt{3}\,\sigma_2'\right) - \frac{1}{\sqrt{6}}\sigma_5'^{\,2}\sigma_1' + \frac{1}{3\sqrt{6}}\sigma_1'\left(\sigma_1'^{\,2} - 3\sigma_2'^{\,2}\right)
\end{aligned}
\tag{61}
$$

The derivatives of the invariants are as follows:

$$
\begin{aligned}
&\frac{\partial I_1}{\partial p} = 1, \quad \frac{\partial I_1}{\partial \sigma_i'} = 0, \quad i = 1,\ldots,5 && \frac{\partial J_1}{\partial p} = 0, \quad \frac{\partial J_1}{\partial \sigma_i'} = 0, \quad \forall i = 1,\ldots,5 \\
&\frac{\partial I_2}{\partial p} = -6p, \quad \frac{\partial I_2}{\partial \sigma_i'} = \sigma_i', \quad i = 1,\ldots,5 && \frac{\partial J_2}{\partial p} = 0, \quad \frac{\partial J_2}{\partial \sigma_i'} = \sigma_i', \quad \forall i = 1,\ldots,5 \\
&\frac{\partial I_3}{\partial p} = -\frac{1}{\sqrt{3}}\left(I_2 + 2p^2\right) = \frac{1}{\sqrt{3}}\left(p^2 - \frac{1}{2}\boldsymbol{\sigma}'^{\mathrm{T}}\,\boldsymbol{\sigma}'\right) && \frac{\partial J_3}{\partial p} = \frac{1}{2\sqrt{3}}\boldsymbol{\sigma}'^{\mathrm{T}}\,\boldsymbol{\sigma}' \\
&\frac{\partial I_3}{\partial \sigma_1'} = \frac{1}{2\sqrt{6}}\left(2\sigma_1'^{\,2} - 2\sigma_2'^{\,2} + \sigma_3'^{\,2} + \sigma_4'^{\,2} - 2\sigma_5'^{\,2}\right) - \frac{1}{\sqrt{3}}p\sigma_1' && \frac{\partial J_3}{\partial \sigma_1'} = \frac{1}{2\sqrt{6}}\left(2\sigma_1'^{\,2} - 2\sigma_2'^{\,2} + \sigma_3'^{\,2} + \sigma_4'^{\,2} - 2\sigma_5'^{\,2}\right) \\
&\frac{\partial I_3}{\partial \sigma_2'} = \frac{1}{2\sqrt{2}}\left(\sigma_3'^{\,2} - \sigma_4'^{\,2}\right) - \frac{\sigma_2'}{\sqrt{3}}\left(p + \sqrt{2}\,\sigma_1'\right) && \frac{\partial J_3}{\partial \sigma_2'} = \frac{1}{2\sqrt{2}}\left(\sigma_3'^{\,2} - \sigma_4'^{\,2}\right) - \sqrt{\frac{2}{3}}\sigma_1'\sigma_2' \\
&\frac{\partial I_3}{\partial \sigma_3'} = \frac{1}{\sqrt{2}}\sigma_4'\sigma_5' - \frac{\sigma_3'}{\sqrt{6}}\left(\sqrt{2}\,p - \sigma_1' - \sqrt{3}\,\sigma_2'\right) && \frac{\partial J_3}{\partial \sigma_3'} = \frac{1}{\sqrt{2}}\sigma_4'\sigma_5' + \frac{\sigma_3'}{\sqrt{6}}\left(\sigma_1' + \sqrt{3}\,\sigma_2'\right) \\
&\frac{\partial I_3}{\partial \sigma_4'} = \frac{1}{\sqrt{2}}\sigma_3'\sigma_5' - \frac{\sigma_4'}{\sqrt{6}}\left(\sqrt{2}\,p - \sigma_1' + \sqrt{3}\,\sigma_2'\right) && \frac{\partial J_3}{\partial \sigma_4'} = \frac{1}{\sqrt{2}}\sigma_3'\sigma_5' + \frac{\sigma_4'}{\sqrt{6}}\left(\sigma_1' - \sqrt{3}\,\sigma_2'\right) \\
&\frac{\partial I_3}{\partial \sigma_5'} = \frac{1}{\sqrt{2}}\sigma_3'\sigma_4' - \frac{\sigma_5'}{\sqrt{6}}\left(\sqrt{2}\,p + 2\sigma_1'\right) && \frac{\partial J_3}{\partial \sigma_5'} = \frac{1}{\sqrt{2}}\sigma_3'\sigma_4' - \frac{2}{\sqrt{6}}\sigma_1'\sigma_5'
\end{aligned}
\tag{62}
$$

B. Rotation matrices

A second-order tensor $\boldsymbol{A}$ transforms by an orthonormal transformation tensor $\boldsymbol{R}$ as

$$
\widehat{\boldsymbol{A}} = \boldsymbol{R}^{\mathrm{T}}\cdot\boldsymbol{A}\cdot\boldsymbol{R} \quad \text{or} \quad \widehat{A}_{kl} = R_{ik}R_{jl}A_{ij}. \tag{63}
$$

In the cartesian orthonormal basis, $\boldsymbol{R} = R_{ij}\boldsymbol{e}_i \otimes \boldsymbol{e}_j$, and coefficients R_{ij} can be arranged in a 3x3 matrix $\mathbf{R}$ as

$$
\mathbf{R} = \begin{pmatrix} R_{11} & R_{12} & R_{13} \\ R_{21} & R_{22} & R_{23} \\ R_{31} & R_{32} & R_{33} \end{pmatrix} \tag{64}
$$

The tensors $\boldsymbol{A}$ and $\widehat{\boldsymbol{A}}$ are expressed in the Voigt notation as $\mathbf{a}$ and $\widehat{\mathbf{a}}$, and then $\widehat{\mathbf{a}} = \mathscr{R}^{\mathrm{T}}\mathbf{a}$, where $\mathscr{R}$ is a 6x6 matrix. Due to the existence of dual bases in the Voigt notation, it follows that if $\mathbf{a}$ is a stress-like (contravariant) tensor, then $\mathscr{R} = \mathscr{R}_{\sigma}^{V}$

$$\mathscr{R}^V_\sigma = \begin{pmatrix} R_{11}^2 & R_{12}^2 & R_{13}^2 & 2R_{12}R_{13} & 2R_{11}R_{13} & 2R_{11}R_{12} \\ R_{21}^2 & R_{22}^2 & R_{23}^2 & 2R_{22}R_{23} & 2R_{21}R_{23} & 2R_{21}R_{22} \\ R_{31}^2 & R_{32}^2 & R_{33}^2 & 2R_{32}R_{33} & 2R_{31}R_{33} & 2R_{31}R_{32} \\ R_{21}R_{31} & R_{22}R_{32} & R_{23}R_{33} & R_{22}R_{33}+R_{23}R_{32} & R_{21}R_{33}+R_{23}R_{31} & R_{21}R_{32}+R_{22}R_{31} \\ R_{11}R_{31} & R_{12}R_{32} & R_{13}R_{33} & R_{12}R_{33}+R_{13}R_{32} & R_{11}R_{33}+R_{13}R_{31} & R_{11}R_{32}+R_{12}R_{31} \\ R_{11}R_{21} & R_{12}R_{22} & R_{13}R_{23} & R_{12}R_{23}+R_{13}R_{22} & R_{11}R_{23}+R_{13}R_{21} & R_{11}R_{22}+R_{12}R_{21} \end{pmatrix} \tag{65}$$

If **a** represents a strain-like (covariant) tensor, then $\mathscr{R} = \mathscr{R}^V_\varepsilon$ and

$$\mathscr{R}^V_\varepsilon = \begin{pmatrix} R_{11}^2 & R_{12}^2 & R_{13}^2 & R_{12}R_{13} & R_{11}R_{13} & R_{11}R_{12} \\ R_{21}^2 & R_{22}^2 & R_{23}^2 & R_{22}R_{23} & R_{21}R_{23} & R_{21}R_{22} \\ R_{31}^2 & R_{32}^2 & R_{33}^2 & R_{32}R_{33} & R_{31}R_{33} & R_{31}R_{32} \\ 2R_{21}R_{31} & 2R_{22}R_{32} & 2R_{23}R_{33} & R_{22}R_{33}+R_{23}R_{32} & R_{21}R_{33}+R_{23}R_{31} & R_{21}R_{32}+R_{22}R_{31} \\ 2R_{11}R_{31} & 2R_{12}R_{32} & 2R_{13}R_{33} & R_{12}R_{33}+R_{13}R_{32} & R_{11}R_{33}+R_{13}R_{31} & R_{11}R_{32}+R_{12}R_{31} \\ 2R_{11}R_{21} & 2R_{12}R_{22} & 2R_{13}R_{23} & R_{12}R_{23}+R_{13}R_{22} & R_{11}R_{23}+R_{13}R_{21} & R_{11}R_{22}+R_{12}R_{21} \end{pmatrix} \tag{66}$$

In the Mandel notation, $\mathscr{R} = \mathscr{R}^M$ for both type of tensors and reads

$$\mathscr{R}^M = \begin{pmatrix} R_{11}^2 & R_{12}^2 & R_{13}^2 & \sqrt{2}R_{12}R_{13} & \sqrt{2}R_{11}R_{13} & \sqrt{2}R_{11}R_{12} \\ R_{21}^2 & R_{22}^2 & R_{23}^2 & \sqrt{2}R_{22}R_{23} & \sqrt{2}R_{21}R_{23} & \sqrt{2}R_{21}R_{22} \\ R_{31}^2 & R_{32}^2 & R_{33}^2 & \sqrt{2}R_{32}R_{33} & \sqrt{2}R_{31}R_{33} & \sqrt{2}R_{31}R_{32} \\ \sqrt{2}R_{21}R_{31} & \sqrt{2}R_{22}R_{32} & \sqrt{2}R_{23}R_{33} & R_{22}R_{33}+R_{23}R_{32} & R_{21}R_{33}+R_{23}R_{31} & R_{21}R_{32}+R_{22}R_{31} \\ \sqrt{2}R_{11}R_{31} & \sqrt{2}R_{12}R_{32} & \sqrt{2}R_{13}R_{33} & R_{12}R_{33}+R_{13}R_{32} & R_{11}R_{33}+R_{13}R_{31} & R_{11}R_{32}+R_{12}R_{31} \\ \sqrt{2}R_{11}R_{21} & \sqrt{2}R_{12}R_{22} & \sqrt{2}R_{13}R_{23} & R_{12}R_{23}+R_{13}R_{22} & R_{11}R_{23}+R_{13}R_{21} & R_{11}R_{22}+R_{12}R_{21} \end{pmatrix} \tag{67}$$

In the natural notation, $\mathscr{R}$ reads

$$\mathscr{R} = \begin{pmatrix} 1 & 0 & 0 & 0 & 0 & 0 \\ 0 & \left(3R_{33}^2-1\right)/2 & \sqrt{3}\left(R_{32}^2-R_{31}^2\right)/2 & \sqrt{3}R_{32}R_{33} & \sqrt{3}R_{31}R_{33} & \sqrt{3}R_{31}R_{32} \\ 0 & \sqrt{3}\left(R_{23}^2-R_{13}^2\right)/2 & \left(R_{11}^2+R_{22}^2-R_{12}^2-R_{21}^2\right)/2 & R_{22}R_{23}-R_{12}R_{13} & R_{23}R_{21}-R_{13}R_{11} & R_{21}R_{22}-R_{11}R_{12} \\ 0 & \sqrt{3}R_{23}R_{33} & R_{22}R_{32}-R_{21}R_{31} & R_{22}R_{33}+R_{23}R_{32} & R_{21}R_{33}+R_{23}R_{31} & R_{22}R_{31}+R_{21}R_{32} \\ 0 & \sqrt{3}R_{13}R_{33} & R_{32}R_{12}-R_{31}R_{11} & R_{12}R_{33}+R_{13}R_{32} & R_{11}R_{33}+R_{13}R_{31} & R_{12}R_{31}+R_{11}R_{32} \\ 0 & \sqrt{3}R_{13}R_{23} & R_{12}R_{22}-R_{11}R_{21} & R_{12}R_{23}+R_{13}R_{22} & R_{11}R_{23}+R_{13}R_{21} & R_{11}R_{22}+R_{12}R_{21} \end{pmatrix} \tag{68}$$

Given a 6x6 matrix $\mathscr{R}$, the proper 3x3 rotation matrix **R** can be inversely calculated as

$$R_{33} = \sqrt{\frac{2\mathscr{R}_{22}+1}{3}}$$

$$R_{32} = \frac{\mathscr{R}_{24}}{\sqrt{3}R_{33}} = \frac{\mathscr{R}_{24}}{\sqrt{2\mathscr{R}_{22}+1}}$$

$$R_{23} = \frac{\mathscr{R}_{42}}{\sqrt{3}R_{33}} = \frac{\mathscr{R}_{42}}{\sqrt{2\mathscr{R}_{22}+1}}$$

$$R_{31} = \frac{\mathscr{R}_{25}}{\sqrt{3}R_{33}} = \frac{\mathscr{R}_{25}}{\sqrt{2\mathscr{R}_{22}+1}}$$

$$R_{13} = \frac{\mathscr{R}_{52}}{\sqrt{3}R_{33}} = \frac{\mathscr{R}_{52}}{\sqrt{2\mathscr{R}_{22}+1}}$$

$$R_{22} = \frac{1}{R_{33}}\left(\mathscr{R}_{44}-R_{23}R_{32}\right) = \sqrt{\frac{3}{2\mathscr{R}_{22}+1}}\left(\mathscr{R}_{44}-\frac{\mathscr{R}_{42}\mathscr{R}_{24}}{2\mathscr{R}_{22}+1}\right)$$

$$R_{11} = \frac{1}{R_{33}}\left(\mathscr{R}_{55}-R_{13}R_{31}\right) = \sqrt{\frac{3}{2\mathscr{R}_{22}+1}}\left(\mathscr{R}_{55}-\frac{\mathscr{R}_{52}\mathscr{R}_{25}}{2\mathscr{R}_{22}+1}\right)$$

$$R_{12} = \frac{1}{R_{13}}\left(R_{22}R_{23}-\mathscr{R}_{34}\right) = \sqrt{\frac{3}{2\mathscr{R}_{22}+1}}\left(\mathscr{R}_{44}-\frac{\mathscr{R}_{42}\mathscr{R}_{24}}{2\mathscr{R}_{22}+1}\right)\frac{\mathscr{R}_{42}}{\mathscr{R}_{52}} - \frac{\mathscr{R}_{34}}{\mathscr{R}_{52}}\sqrt{2\mathscr{R}_{22}+1}$$

$$R_{21} = \frac{1}{R_{31}}(R_{22}R_{32} - \mathscr{R}_{43}) = \sqrt{\frac{3}{2\mathscr{R}_{22}+1}}\left(\mathscr{R}_{44} - \frac{\mathscr{R}_{24}\mathscr{R}_{42}}{2\mathscr{R}_{22}+1}\right)\frac{\mathscr{R}_{24}}{\mathscr{R}_{25}} - \frac{\mathscr{R}_{43}}{\mathscr{R}_{25}}\sqrt{2\mathscr{R}_{22}+1}$$

For the sake of completeness, some important remarks on the update of the rotation matrix are given in the following.
Given a spin tensor represented as a skew-symmetric matrix

$$\mathbf{W} = \begin{pmatrix} 0 & -w_3 & w_2 \\ w_3 & 0 & -w_1 \\ -w_2 & w_1 & 0 \end{pmatrix}, \tag{70}$$

in which w_1, w_2, w_3 are components of spin vector $\mathbf{w}$, the update of the rotation matrix $\mathbf{R}$ is given by the differential equation

$$\dot{\mathbf{R}} = \mathbf{W}\,\mathbf{R}. \tag{71}$$

Analytical solution exists for the case of constant $\mathbf{W}$ and can be written using Euler-Rodriguez formula as

$$\mathbf{R}(t) = \left(\mathbf{I} + \frac{\sin(wt)}{w}\mathbf{W} + \frac{(1-\cos(wt))}{w^2}\mathbf{W}\mathbf{W}\right)\mathbf{R}_0 \tag{72}$$

where $\mathbf{R}_0 = \mathbf{R}(0)$ and $w = \sqrt{w_1^2 + w_2^2 + w_3^2}$. In general, the spin $\mathbf{W}$ is a function of time. Eq (71) is then applied per time increment Δt as

$$\mathbf{R}_{n+1} = \Delta\mathbf{R}\,\mathbf{R}_n = \left(\mathbf{I} + \frac{\sin(w_n\Delta t)}{w_n}\mathbf{W}_n + \frac{(1-\cos(w_n\Delta t))}{w_n^2}\mathbf{W}_n\mathbf{W}_n\right)\mathbf{R}_n \tag{73}$$

The symmetric numerical second-order update scheme by Hughes and Winget (1980) is often employed (e.g. DROT rotation increment matrix in UMAT in Abaqus/Standard), which assumes that the spin $\mathbf{W}$ is known at time $t_{n+1/2} = t_n + \frac{1}{2}\Delta t$. It reads (using Cayley's formula (Cayley, 1846) in order to avoid solving the matrix inverse)

$$\mathbf{R}_{n+1} = \left(\mathbf{I} - \frac{\Delta t}{2}\mathbf{W}_{n+\frac{1}{2}}\right)^{-1}\left(\mathbf{I} + \frac{\Delta t}{2}\mathbf{W}_{n+\frac{1}{2}}\right)\mathbf{R}_n = \left(\mathbf{I} + \frac{\Delta t}{1 + \frac{\Delta t^2}{4}\mathbf{W}_{n+\frac{1}{2}} : \mathbf{W}_{n+\frac{1}{2}}}\left(\mathbf{W}_{n+\frac{1}{2}} + \frac{\Delta t}{2}\mathbf{W}_{n+\frac{1}{2}}\,\mathbf{W}_{n+\frac{1}{2}}\right)\right)\mathbf{R}_n \tag{74}$$

The 6x6 matrix $\mathscr{R}_{n+1}$ needs then to be built by using Eq. (68).

C. *Elastic stiffness tensor for orthotropic symmetry*

The elastic stiffness matrix for orthotropic symmetry is written in Voigt notation as

$$\mathbf{C}^V_{\text{orth}} = \begin{pmatrix} C_{11} & C_{12} & C_{13} & 0 & 0 & 0 \\ C_{12} & C_{22} & C_{23} & 0 & 0 & 0 \\ C_{13} & C_{23} & C_{33} & 0 & 0 & 0 \\ 0 & 0 & 0 & C_{44} & 0 & 0 \\ 0 & 0 & 0 & 0 & C_{55} & 0 \\ 0 & 0 & 0 & 0 & 0 & C_{66} \end{pmatrix} \tag{75}$$

It transforms using the new notation into $\mathbf{C}_{orth}$ with the non-zero components (the super-script "V" denoting the Voigt notation in C_{ij} coefficients are omitted) as

$$\begin{aligned}
C_{11} &:= \frac{1}{3}(C_{11} + C_{22} + C_{33} + 2C_{23} + 2C_{13} + 2C_{12}) \\
C_{12} &:= \frac{1}{3\sqrt{2}}(-C_{11} - C_{22} + 2C_{33} + C_{23} + C_{13} - 2C_{12}) \\
C_{13} &:= \frac{1}{\sqrt{6}}(-C_{11} + C_{22} + C_{23} - C_{13}) \\
C_{22} &:= \frac{1}{6}(C_{11} + C_{22} + 4C_{33} - 4C_{23} - 4C_{13} + 2C_{12}) \\
C_{23} &:= \frac{1}{2\sqrt{3}}(C_{11} - C_{22} + 2C_{23} - 2C_{13}) \\
C_{33} &:= \frac{1}{2}(C_{11} + C_{22} - 2C_{12})
\end{aligned} \tag{76}$$

and

$$C_{44} := 2C_{44} \quad C_{55} := 2C_{55} \quad C_{66} := 2C_{66}$$

D. Transformation of the Hessian

The Hessian expressed in the natural notation reads

$$\mathbf{H}=\frac{1}{2}\begin{pmatrix} 0 & 0 & 0 & 0 & 0 & 0 \\ & 3(H_{1111}+2H_{1122}+H_{2222}) & \sqrt{3}(H_{1111}-H_{2222}) & -\sqrt{3}(H_{1123}+H_{2223}) & -\sqrt{3}(H_{1113}+H_{2213}) & -\sqrt{3}(H_{1112}+H_{2212}) \\ & & H_{1111}-2H_{1122}+H_{2222} & -H_{1123}+H_{2223} & -H_{1113}+H_{2213} & -H_{1112}+H_{2212} \\ & & & H_{2323} & H_{2313} & H_{2312} \\ & & \text{symmetric} & & H_{1313} & H_{1312} \\ & & & & & H_{1212} \end{pmatrix} \tag{77}$$

E. Relations of anisotropy coefficients between Yld2004, Yld91 and Hill48

As can be seen from Eq. (37), Yld2004 reduces into Yld91 when relations apply as

$$\begin{aligned} L_{22} &= \left(\overline{a}+\overline{b}\right)\Big/2, \\ L_{23}=L_{32} &= \frac{\sqrt{3}}{6}\left(\overline{b}-\overline{a}\right), \\ L_{33} &= \left(\overline{a}+\overline{b}+4\overline{c}\right)\Big/6, \\ L_{12}=L_{13} &= 0 \\ L_{44}=\overline{f}\Big/2, &\quad L_{55}=\overline{g}\Big/2, \quad L_{66}=\overline{h}\Big/2 \end{aligned} \tag{78}$$

The inverse relations read

$$\begin{aligned} &\overline{a}=L_{22}-\sqrt{3}L_{23}, \\ &\overline{b}=L_{22}+\sqrt{3}L_{23}, \\ &\overline{c}=(3L_{33}-L_{22})/2, \\ &\overline{f}=2L_{44}, \quad \overline{g}=2L_{55}, \quad \overline{h}=2L_{66} \end{aligned} \tag{79}$$

For exponent $a=2$, Yld91 equals to Hill48 and the link between their coefficients is as

$$\begin{aligned} F &= \frac{1}{6}\left(2\overline{a}^2+\overline{a}\overline{b}+\overline{a}\overline{c}-\overline{b}\overline{c}\right)=\frac{1}{2}L_{23}^2+\frac{1}{2}L_{22}^2-\frac{\sqrt{3}}{2}(L_{22}+L_{33})L_{23} \\ G &= \frac{1}{6}\left(2\overline{b}^2+\overline{a}\overline{b}-\overline{a}\overline{c}+\overline{b}\overline{c}\right)=\frac{1}{2}L_{23}^2+\frac{1}{2}L_{22}^2+\frac{\sqrt{3}}{2}(L_{22}+L_{33})L_{23} \\ H &= \frac{1}{6}\left(2\overline{c}^2-\overline{a}\overline{b}+\overline{a}\overline{c}+\overline{b}\overline{c}\right)=\frac{1}{4}\left(2L_{23}^2+3L_{33}^2-L_{22}^2\right) \\ L &= \frac{3}{8}\overline{f}^2=\frac{3}{2}L_{44}^2, \quad M=\frac{3}{8}\overline{g}^2=\frac{3}{2}L_{55}^2, \quad N=\frac{3}{8}\overline{h}^2=\frac{3}{2}L_{66}^2 \end{aligned} \tag{80}$$

To be reminded, $L_{ij}-$ coefficients are anisotropy coefficients of Yld2004-18p when the natural vector notation is employed for the stress. For completeness, if the Voigt notation is used, the relations in Eq. (78) become

$$\begin{aligned} F &= \frac{1}{18}\left(-2C_{12}^2-C_{12}C_{23}-7C_{31}C_{12}+10C_{23}^2+5C_{31}C_{23}+4C_{31}^2\right) \\ G &= \frac{1}{18}\left(4C_{12}^2-7C_{12}C_{23}+5C_{31}C_{12}-2C_{23}^2-C_{31}C_{23}+10C_{31}^2\right) \\ H &= \frac{1}{18}\left(10C_{12}^2+5C_{12}C_{23}-C_{31}C_{12}+4C_{23}^2-7C_{31}C_{23}-2C_{31}^2\right) \\ L &= \frac{3}{2}C_{44}^2, \quad M=\frac{3}{2}C_{55}^2, \quad N=\frac{3}{2}C_{66}^2 \end{aligned} \tag{81}$$

The remaining coefficients C_{21}, C_{13} and C_{32} must obey

$$\begin{aligned} C_{13} &= (2C_{31}+2C_{12}-C_{23})/3 \\ C_{32} &= (2C_{23}+2C_{31}-C_{12})/3 \\ C_{21} &= (2C_{12}+2C_{23}-C_{31})/3 \end{aligned} \tag{82}$$

References

Aretz, H., Aegerter, J., Engler, O., 2010. Analysis of earing in deep drawn cups. Aip. Conf. Proc. 1252, 417–424.

Aretz, H., Barlat, F., 2013. New convex yield functions for orthotropic metal plasticity, 51, 97–111.

Auffray, N., Le Quang, H., He, Q.C., 2013. Matrix representations for 3D strain-gradient elasticity, 61, 1202–1223.

Barlat, F., Aretz, H., Yoon, J.W., Karabin, M.E., Brem, J.C., Dick, R.E., 2005. Linear transfomation-based anisotropic yield functions. Int. J. Plast. 21, 1009–1039.
Barlat, F., Brem, J.C., Yoon, J.W., Chung, K., Dick, R.E., Lege, D.J., Pourboghrat, F., Choi, S.H., Chu, E., 2003. Plane stress yield function for aluminum alloy sheets—part 1: theory. Int. J. Plast. 19, 1297–1319.
Barlat, F., Lege, D.J., Brem, J.C., 1991. A six-component yield function for anisotropic materials. Int. J. Plast. 7, 693–712.
Barlat, F., Yoon, J.W., Cazacu, O., 2007. On linear transformations of stress tensors for the description of plastic anisotropy. Int. J. Plast. 23, 876–896.
Becker, R., 2011. An alternative approach to integrating plasticity relations. Int. J. Plast. 27, 1224–1238.
Bishop, J.W.F., Hill, R., 1951. A theoretical derivation of plastic properties of a polycrystalline face-centered metal. Phil. Mag. 42, 1298–1307.
Boehler, J.P., Sawczuk, A., 1970. Equilibrium limit of anisotropic soils. J. Mec. 9, 5–&.
Brannon, R.M., 2018. Rotation, Reflection, and Frame Changes, Orthogonal Tensors in Computational Engineering Mechanics. IOP Publishing.
Canova, G.R., Kocks, U.F., Tome, C.N., Jonas, J.J., 1985. The yield surface of textured polycrystals. J. Mech. Phys. Solid. 33, 371–397.
Cayley, A., 1846. Sur quelques propriétés des déterminants gauches. J. für die Reine Angewandte Math. (Crelle's J.) 1846, 119.
Cazacu, O., 2019. New mathematical results and explicit expressions in terms of the stress components of Barlat et al. (1991) orthotropic yield criterion. Int. J. Solid Struct. 176–177, 86–95.
Choi, H., Yoon, J.W., 2019. Stress integration-based on finite difference method and its application for anisotropic plasticity and distortional hardening under associated and non-associated flow rules. Comput. Methods Appl. Mech. Eng. 345, 123–160.
Crumbach, M., Pomana, G., Wagner, P., Gottstein, G., 2001. A Taylor Type Deformation Texture Model Considering Grain Interaction and Material Properties. Part I - Fundamentals. Springer-Verlag Berlin, Berlin.
De Borst, R., Feenstra, P.H., 1990. Studies in anisotropic plasticity with reference to the Hill criterion. Int. J. Numer. Methods Eng. 29, 315–336.
Dunne, F., Petrinic, N., 2006. Introduction to Computational Plasticity. Oxford University Press.
Goldstein, A., 1965. On Steepest Descent.
Grilo, T.J., Valente, R.A.F., de Sousa, R.J.A., 2014. Assessment on the performance of distinct stress integration algorithms for complex non-quadratic anisotropic yield criteria. Int. J. Material Form. 7, 233–247.
Helnwein, P., 2001. Some remarks on the compressed matrix representation of symmetric second-order and fourth-order tensors, 190, 2753–2770.
Hill, R., 1948. A theory of the yielding and plastic flow of anisotropic metals. Proc R Soc Lon Ser-A 193, 281–297.
Hosford, W.F., 1972. A generalized isotropic yield criterion. J. Appl. Mech. 39, 607–609.
Hughes, T.J.R., 1984. Numerical implementation of constitutive models: rate-independent deviatoric plasticity. In: Nemat-Nasser, S., Asaro, R.J., Hegemier, G.A. (Eds.), Theoretical Foundation for Large-Scale Computations for Nonlinear Material Behavior: Proceedings of the Workshop on the Theoretical Foundation for Large-Scale Computations of Nonlinear Material Behavior Evanston, Illinois, October 24, 25, and 26, 1983. Springer Netherlands, Dordrecht, pp. 29–63.
Hughes, T.J.R., Winget, J., 1980. Finite rotation effects in numerical-integration of rate constitutive-equations arising in large-deformation analysis. Int. J. Numer. Methods Eng. 15, 1862–1867.
Karafillis, A.P., Boyce, M.C., 1993. A general anisotropic yield criterion using bounds and a transformation weighting tensor. J. Mech. Phys. Solid. 41, 1859–1886.
Kocks, U.F., Canova, G., Tome, C., Rollett, A.D., Wright, S.I., 1995. LApp - Los Alamos Polycrystal Plasticity Simulation Code, 8 ed. Los Alamos, New Mexico, USA, Version 6.
Kocks, U.F., Canova, G.R., Jonas, J.J., 1983. Yield vectors in fcc crystals. Acta Metall. 31, 1243–1252.
Kocks, U.F., Tome, C., Wenk, H.-R., 1998. Texture and Anisotropy. In: Preferred Orientations in Polycrystals and Their Effect on Materials Properties. Cambridge University Press, Cambridge.
Kojić, M., 2002. Stress integration procedures for inelastic material models within the Finite Element Method, 55, 389.
Krishnamoorthy, A., Menon, D., 2013. Matrix Inversion Using Cholesky Decomposition, 2013 Signal Processing: Algorithms, Architectures, Arrangements, and Applications (SPA), pp. 70–72.
Lebensohn, R.A., Tomé, C.N., 1993. A self-consistent anisotropic approach for the simulation of plastic deformation and texture development of polycrystals: application to zirconium alloys. Acta Metall. Mater. 41, 2611–2624.
Lee, J., Lee, M.-G., Barlat, F., Kim, J.H., 2012. Stress integration schemes for novel homogeneous anisotropic hardening model, 247–248, 73–92.
Lequeu, P., 1986. Comparison of Crystallographic and Continuum Yield Surfaces for Textured Polycrystals. Department of Mining and Metallurgical Engineering. McGill University.
Lester, B.T., Scherzinger, W.M., 2017. Trust-region based return mapping algorithm for implicit integration of elastic-plastic constitutive models. Int. J. Numer. Methods Eng. 112, 257–282.
Levkovitch, V., Svendsen, B., 2007. Accurate hardening modeling as basis for the realistic simulation of sheet forming processes with complex strain-path changes. In: CeasarDeSa, J.M.A., Santos, A.D. (Eds.), NUMIFORM '07: Materials Processing and Design: Modeling, Simulation and Applications, Pts I and II. Amer Inst Physics, Melville, pp. 1331–1336.
Malvern, L.E., 1969. Introduction to the Mechanics of a Continuous Medium. Prentice-Hall, Englewood Cliffs, N.J.
Mandel, J., 1965. Generalisation de la theorie de plasticite de W. T. Koiter. 1, 273–295.
Mánik, T., Holmedal, B., 2013. Additional relaxations in the Alamel texture model. Mater. Sci. Eng., A 580, 349–354.
Maudlin, P.J., Bingert, J.F., House, J.W., Chen, S.R., 1999. On the modeling of the Taylor cylinder impact test for orthotropic textured materials: experiments and simulations. Int. J. Plast. 15, 139–166.
Moakher, M., 2008. Fourth-order cartesian tensors: old and new facts, notions and applications. Q. J. Mech. Appl. Math. 61, 181–203.
Moran, B., Ortiz, M., Shih, C.F., 1990. Formulation of implicit finite-element methods for multiplicative finite deformation plasticity. Int. J. Numer. Methods Eng. 29, 483–514.
Mosler, J., Bruhns, O.T., 2010. On the implementation of rate-independent standard dissipative solids at finite strain – variational constitutive updates. Comput. Methods Appl. Mech. Eng. 199, 417–429.
Nagtegaal, J.C., 1982. On the implementation of inelastic constitutive equations with special reference to large deformation problems. Comput. Methods Appl. Mech. Eng. 33, 469–484.
Ortiz, M., Popov, E.P., 1985. Accuracy and stability of integration algorithms for elastoplastic constitutive relations. Int. J. Numer. Methods Eng. 21, 1561–1576.
Ortiz, M., Simo, J.C., 1986. An analysis of a new class of integration algorithms for elastoplastic constitutive relations. Int. J. Numer. Methods Eng. 23, 353–366.
Pérez-Foguet, A., Armero, F., 2002. On the formulation of closest-point projection algorithms in elastoplasticity-part II: globally convergent schemes, 53, 331–374.
Scherzinger, W.M., 2017. A return mapping algorithm for isotropic and anisotropic plasticity models using a line search method. Comput. Methods Appl. Math. 317, 526–553.
Scherzinger, W.M., Dohrmann, C.R., 2008. A robust algorithm for finding the eigenvalues and eigenvectors of 3 x 3 symmetric matrices. Comput. Methods Appl. Mech. Eng. 197, 4007–4015.
Simo, J.C., Hughes, T.J.R., 1998. Computational Inelasticity, 1 ed. Springer-Verlag New York, New York.
Simo, J.C., Kennedy, J.G., Govindjee, S., 1988. Non-smooth multisurface plasticity and viscoplasticity. Loading/unloading conditions and numerical algorithms. Int. J. Numer. Methods Eng. 26, 2161–2185.
Simo, J.C., Ortiz, M., 1985. A unified approach to finite deformation elastoplastic analysis based on the use of hyperelastic constitutive equations. Comput. Methods Appl. Mech. Eng. 49, 221–245.
Soare, S.C., Barlat, F., 2011. A study of the Yld2004 yield function and one extension in polynomial form: a new implementation algorithm, modeling range, and earing predictions for aluminum alloy sheets. Eur. J. Mech. Solid. 30, 807–819.
Sobotka, Z., 1969. Theory of plastic flow of anisotropic bodies. Z. Angew. Math. Mech. 49, 25–&.
Taylor, G.I., 1938. Plastic strain in metals. J. Inst. Met. 62, 307–324.
Tomé, C., Kocks, U.F., 1985. The yield surface of h.c. Crystals 33, 603–621.
Tome, C., Lebensohn, R.A., 2009. Manual for Code Visco-Plastic Self-Consistent (VPSC) Version 7c.
van den Boogaard, T., Havinga, J., Belin, A., Barlat, F.J., 2016. Parameter reduction for the Yld2004-18p yield criterion. Int. J. Mater. Form. 9, 175–178.
Van Houtte, P., 1988. A comprehensive mathematical formulation of an extended Taylor-Bishop-hill model featuring relaxed constraints, the Renouard-Wintenberger theory and a strain rate sensitivity model. Textures Microstruct. 8–9, 313–350.
Van Houtte, P., Delannay, L., Samajdar, I., 1999. Quantitative prediction of cold rolling textures in low-carbon steel by means of the Lamel model. Textures Microstruct. 31, 109–149.
Van Houtte, P., Li, S., Seefeldt, M., Delannay, L., 2005. Deformation texture prediction: from the Taylor model to the advanced Lamel model. Int. J. Plast. 21, 589–624.
Versino, D., Bennett, K.C., 2018. Generalized radial-return mapping algorithm for anisotropic von Mises plasticity framed in material eigenspace. Int. J. Numer. Methods Eng. 116, 202–222.
Voigt, W., 1910. Lehrbuch der kristallphysik. Teubner, Leipzig.
Wilkins, M.L., 1969. Calculation of Elasto-Plastic Flow. California Univ., Livermore, p. 101. Lawrence Radiation Lab., p. Medium: X; Size.